

総合地質

General Geology

Vol. 6 No. 1

総説

北海道の文化と石材，特に小樽市とその周辺地域を中心とした文化地質学的検討：松田義章
 A case study on the relation between culture and building stones in Hokkaido, especially culture-geological investigations in the Otaru district: Yoshiaki Matsuda 1-12

論説

三波川変成岩類の上昇：メカニズムとプロセス：君波和雄
 Exhumation of the high P/T Sanbagawa metamorphic rocks: Mechanism and process: Kazuo Kiminami 13-33

北海道登別市のカルルス粘土層の珪藻群集と火山灰組成：嵯峨山 積・井島行夫・荒川昌伸
 Diatom assemblage and volcanic ash composition of the Karurusu Clay Bed in the Noboribetsu, Hokkaido, Japan: Tsumoru Sagayama, Ikuo Izima and Masanobu Arakawa 35-38

西南北海道北部，磯谷地域の新第三紀磯谷層の珪藻生層序：菅原 誠・嵯峨山 積
 Diatom biostratigraphy of the Isoya Formation, Neogene, in Isoya region, northern part of southwestern Hokkaido, Japan: Makoto Sugawara and Tsumoru Sagayama 39-46

北海道倶知安町高砂の法面に現れた古倶知安湖堆積物：井上 隆・関根達夫・岡村 聡・小田桐 亮・嵯峨山 積
 Appearance of the Paleo-Lake Kutchan deposits on the slope of Takasago, Kutchan-cho, Hokkaido, Japan: Takashi Inoue, Tatsuo Sekine, Satoshi Okamura, Ryo Odagiri and Tsumoru Sagayama 47-56

北海道東部然別湖北岸ヤンベツ川下流の後期更新世～完新世の湖沼堆積物と大雪御鉢平カルデラ起源降下火山灰について：岡 孝雄・大西 潤
 Late Pleistocene to Holocene lacustrine deposits and ash fall (Ds-Oh) derived from the Daisetsu-Ohachidaira Caldera around the lower Yanbetsu River, northern coastal area of Lake Shikaribetsu in the eastern Hokkaido: Takao Oka and Jun Ohnishi 57-80

報告・資料

最近の北海道およびその周辺の地震活動 (2018～2021)：高波鐵夫
 Recent seismic activity in and around Hokkaido, Japan (2018-2021): Tetsuo Takanami 81-84

自由投稿

支笏湖南岸「苔の洞門」の洪水史：宮坂省吾
 History of the floods on the southern shore of Lake Shikotsu: Seigo Miyasaka 85-91

論文紹介 93-100

追悼 101

特定非営利活動法人 北海道総合地質学研究センター Hokkaido Research Center of Geology

理事長：宮下純夫 President: Sumio Miyashita

副理事長：嵯峨山 積 Vice President: Tsumoru Sagayama

総合地質 General Geology

編集委員会 Editorial Committee

委員長：宮下純夫 Chief Editor: Sumio Miyashita

副委員長：岡 孝雄 Editor: Takao Oka

委員：君波和雄 Editor: Kazuo Kiminami

委員：松田義章 Editor: Yoshiaki Matsuda

委員：岡村 聡 Editor: Satoshi Okamura

委員：柳下文夫 Editor: Fumio Yagishita

<総説>

北海道の文化と石材，特に小樽市とその周辺地域を中心とした 文化地質学的検討

松田 義章^{1), 2)}

A case study on the relation between culture and building stones in Hokkaido,
especially culture-geological investigations in the Otaru district.

Yoshiaki Matsuda^{1), 2)}

2022年5月1日受付

2022年7月15日受理

1) 北海道総合地質学研究センター

Hokkaido Research Center of Geology,

連絡先：047-0152 小樽市新光3丁目18番7号

Address: 3-18-7, Shinkou, Otaru

2) 北海道教育大学札幌校

002-8502 札幌市北区あいの里5条3丁目1-5

Hokkaido University of Education, Sapporo Campus

5-3-1-5, Ainosato, Kiraku, Sapporo

Corresponding author: songtianyizhang5@gmail.com

Keywords: culture-geology, building stones in Hokkaido, stone circle, ancient lithographs, "Sapporo-Nanseki", "Otaru-Nanseki"

地学団体研究会第71回旭川大会で一部を公表

要旨

北海道の文化史において石材との関わりが大きい文化として、縄文後期、続縄文及び近代の文化の3つの文化を取り上げ、文化と石材との関わりについて検討した。

北海道における「石の文化」は、縄文文化(後期)に石の文化の象徴であるストーン・サークルが本州東北部のそれとは構造が単純化し小型化するなどの変化をとげて、やがて、「土の文化」としての周堤墓へと変化していく分岐点としての特徴を有する。また、続縄文文化のフゴッペ洞窟等における刻画の、ユーラシア大陸北東部ないし本州の「海人」による外来の文化に対して、土着の続縄文文化がそれを許容するような開かれた文化であった。さらに、近代の札幌と小樽における「札幌軟石」や「小樽軟石」の活用の文化が、官庁舎や石造倉庫等の石造建築物を構成する「石の街」の形成に寄与した。

はじめに

小論のテーマにある「文化地質学」について、鈴木(2016)は、「人類の文化が地質とどのように関わってきたかを研究する分野である。」と定義している。また、仁科ほか(2019)は地質と都市景観を融合したジオツーリズムの実施を提唱している。これらの動向を踏まえて、今回、北海道の文化と地質について、特に石材の活用との関わりを切り口として、文化地質学的に検討しレビューすることを試みた。

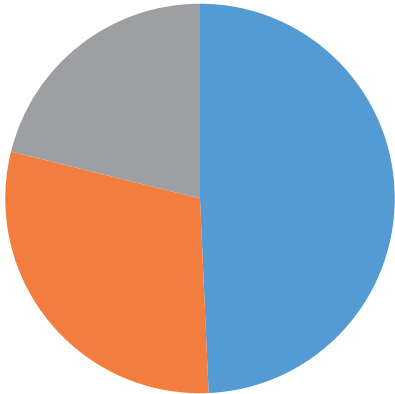
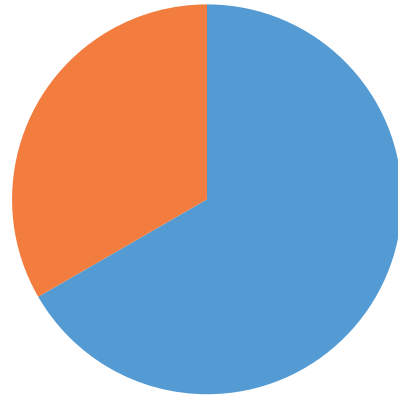
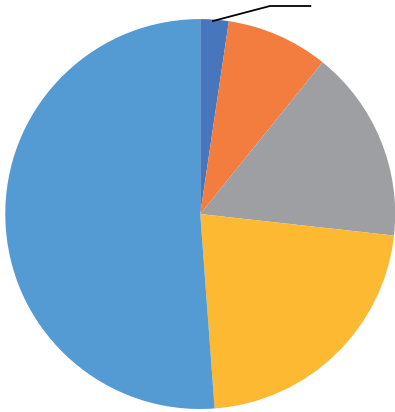
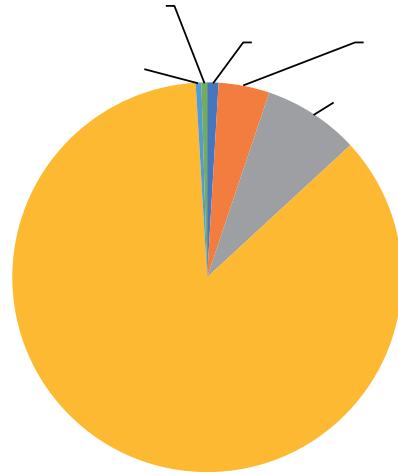
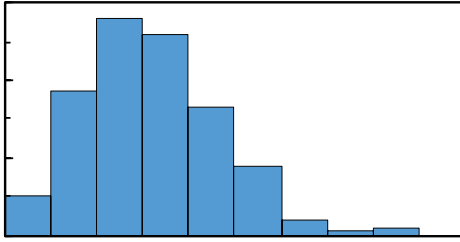
問題の所在についての概観

1. 北海道の文化に関するキーワード

北海道の歴史・文化のキーワードと称すべきものとして、以下のものをあげることができる。旧石器文化、石刃族文化、縄文文化、続縄文文化、擦文文化、オホーツク文化、トビニタイ文化、アイヌ文化、中世(館)文化、近世(松前藩)文化、近代(明治維新)以降の開拓使の文化(H. ケプロン、黒田清隆)や、おもにW. クラークの流れをくむ開拓使仮学校-札幌農学校-東北帝国大学農科大学-北海道帝国大学-北海道大学の系譜をもつ



z, "w =qtP >t-løqfw*%•~>æúq`h =•i¶\$U|







Inscriptions at Otari

(from "NOTES ON STONE IMPLEMENTS FROM OTARI AND HAKODATE, WITH A FEW GENERAL REMARKS ON THE PREHISTORIC REMAINS OF JAPAN," BY JOHN MILNE.)



INSCRIPTIONS AT OTARI











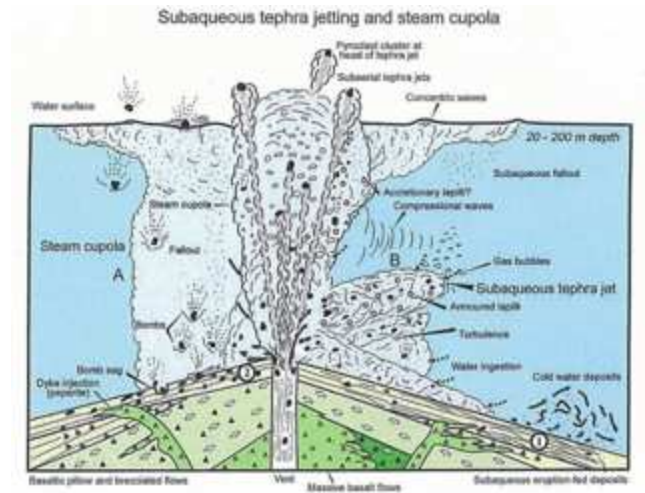


Plate 4. A model for shallow-water, small-volume, Surtsey-type eruptions with continuous open conditions (A) and individual tephra jets (B). (1) lapilli fall; subaqueous eruption-fed density current deposits; (2) lapilli fall breccia; ballistically emplaced pyroclasts forming impact structures under a steam cupola. Diagram not to scale.

Abstract

There are four types of historical artifact and relic of different ages deeply related to stone in Hokkaido: stone tools made from obsidian in the Palaeolithic era, stone circles in the Late Jomon

石器時代の石器、縄文時代の石器、

新石器時代の石器、

縄文時代の石器、

新石器時代の石器、

縄文時代の石器、

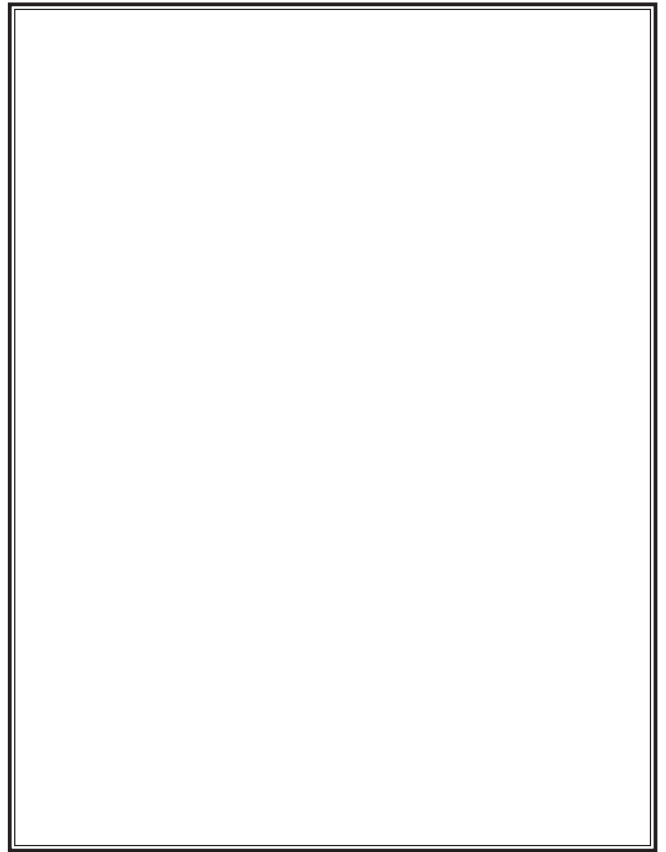
新石器時代の石器、

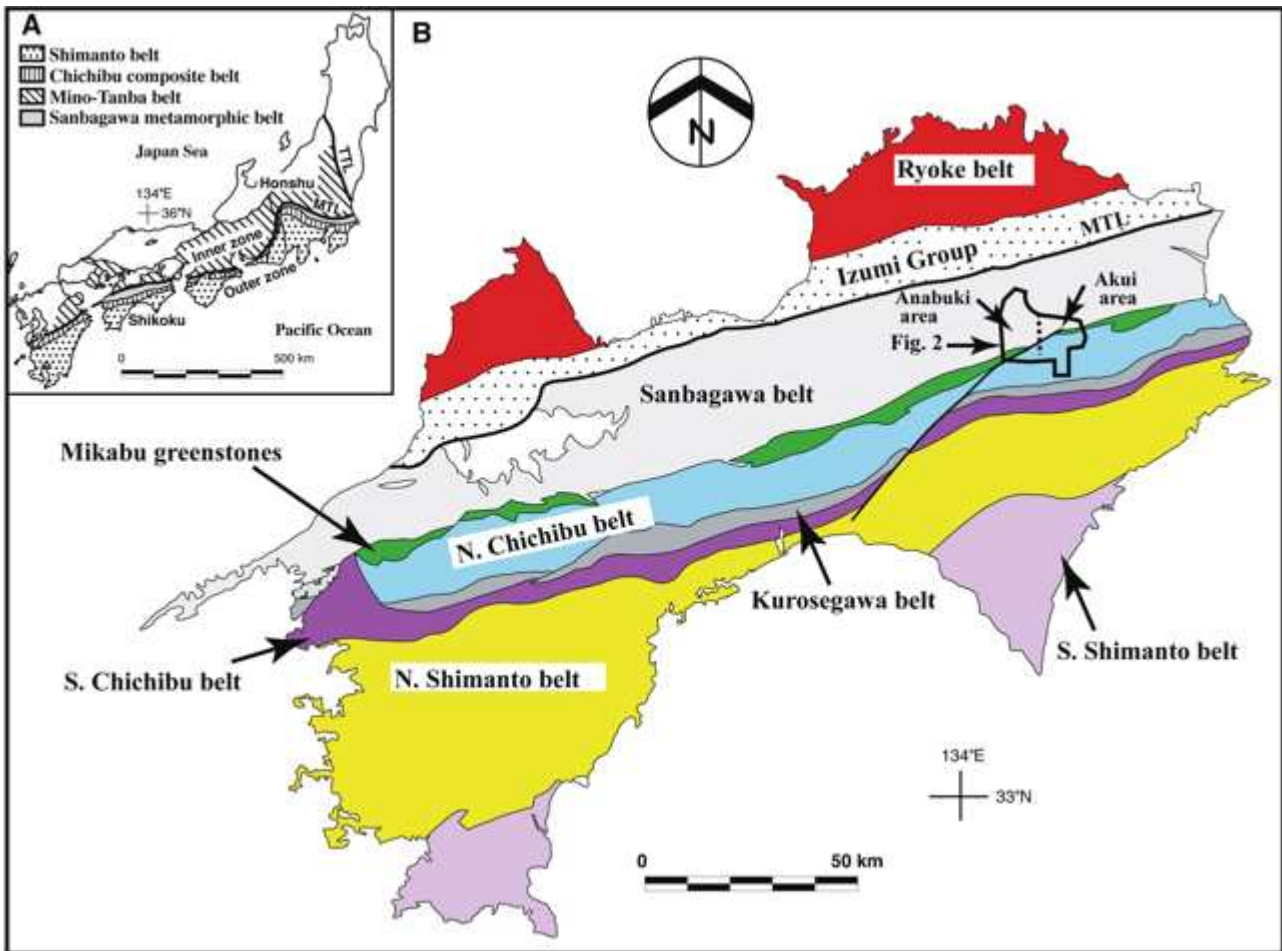
縄文時代の石器、

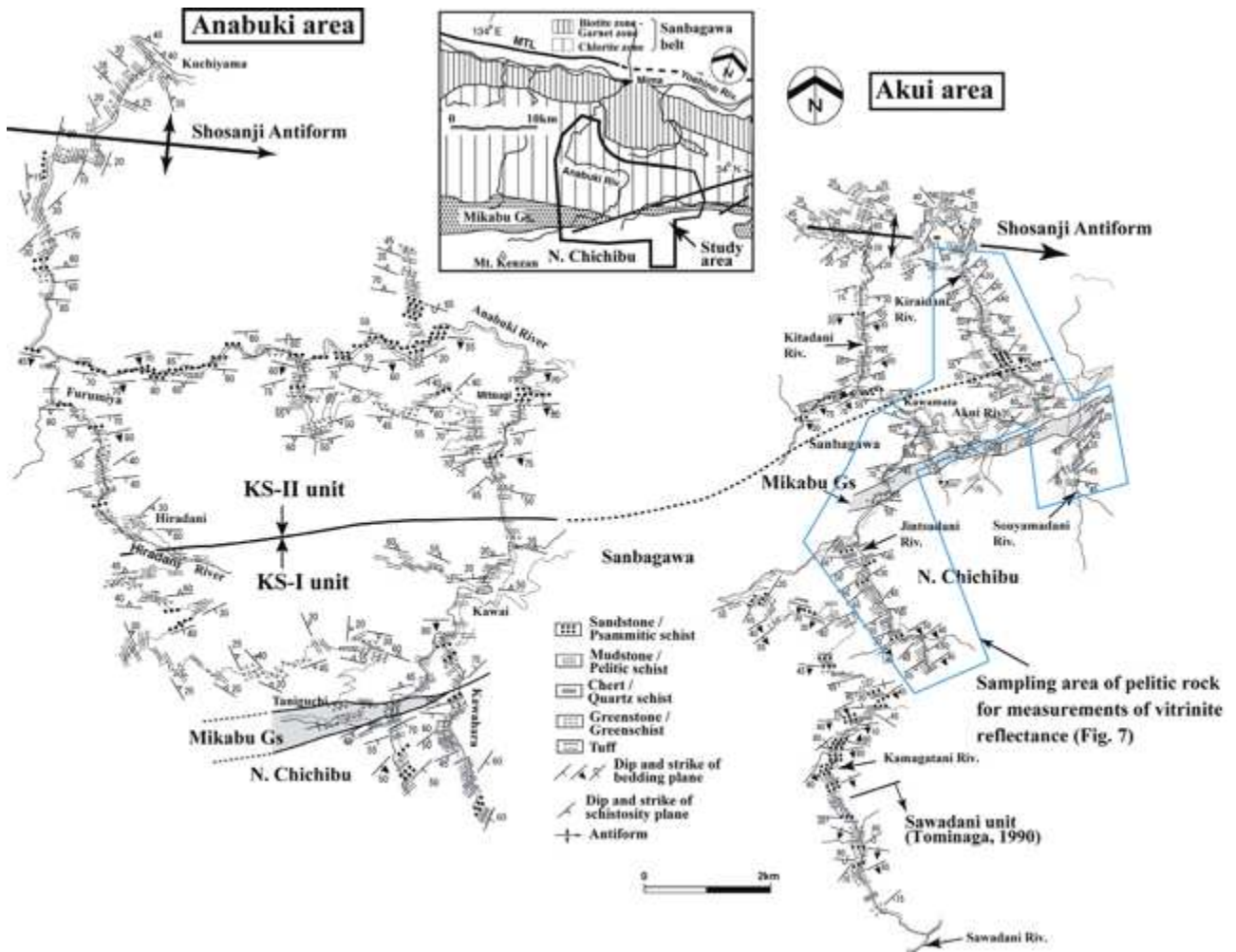
新石器時代の石器、

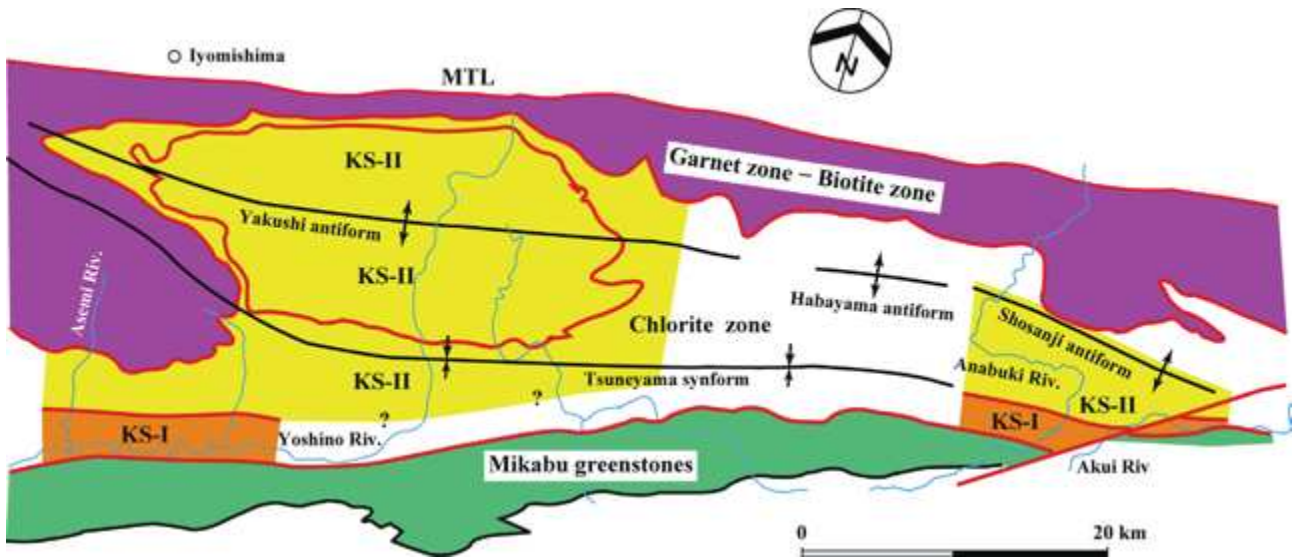
縄文時代の石器、

新石器時代の石器、

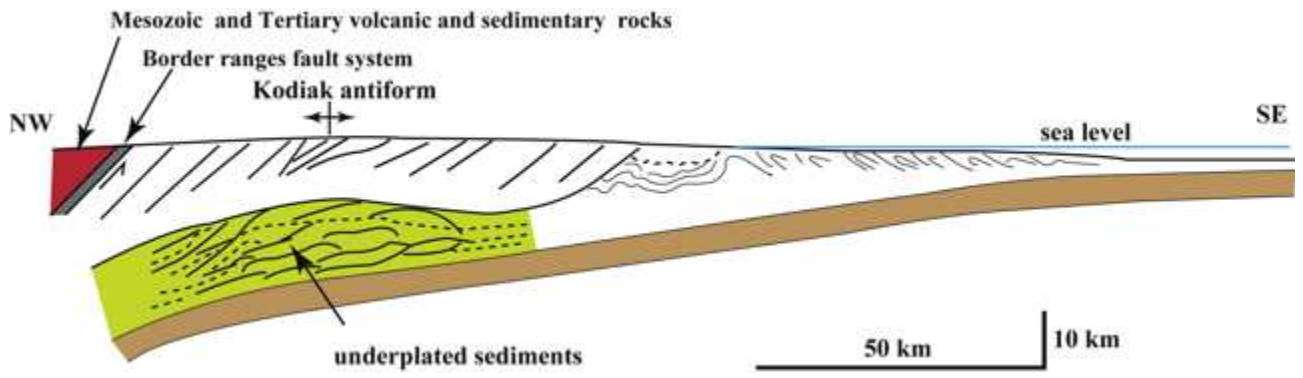




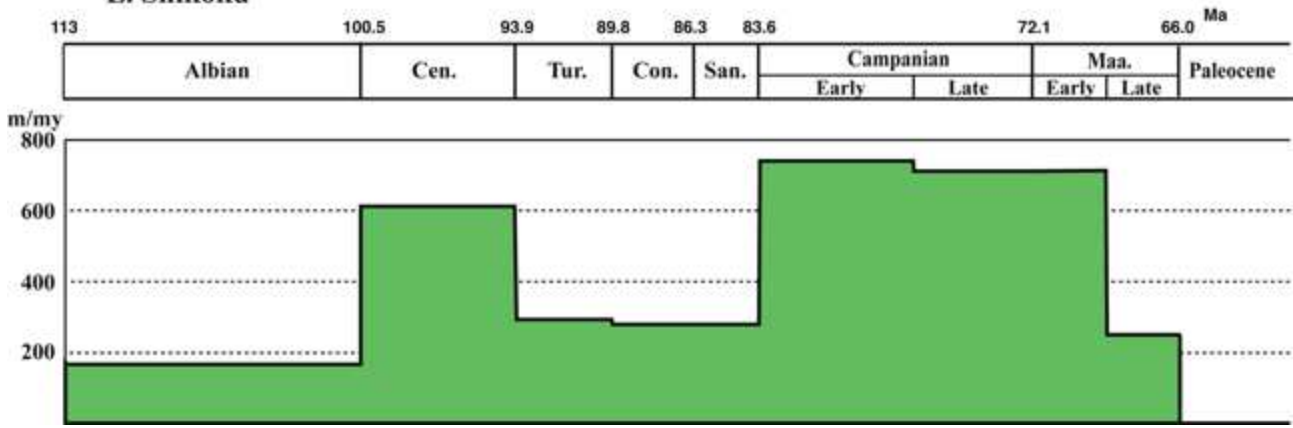


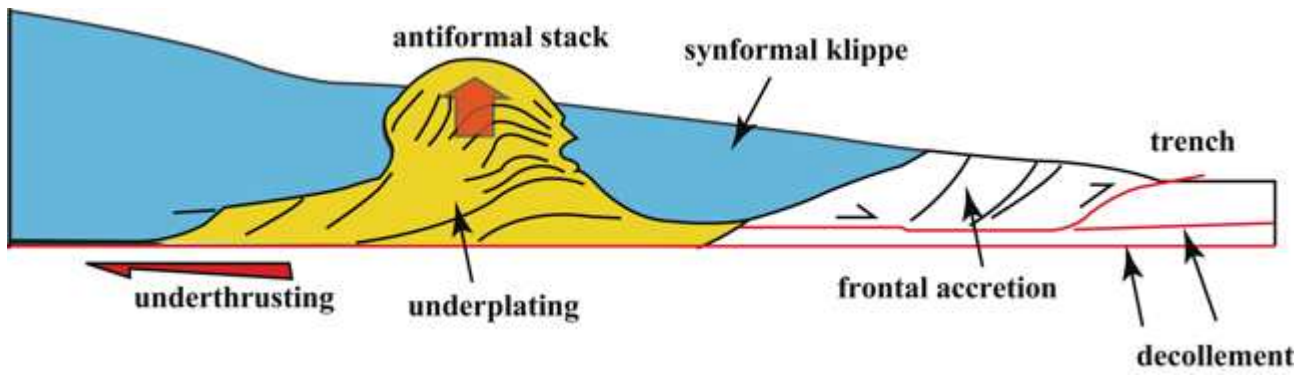


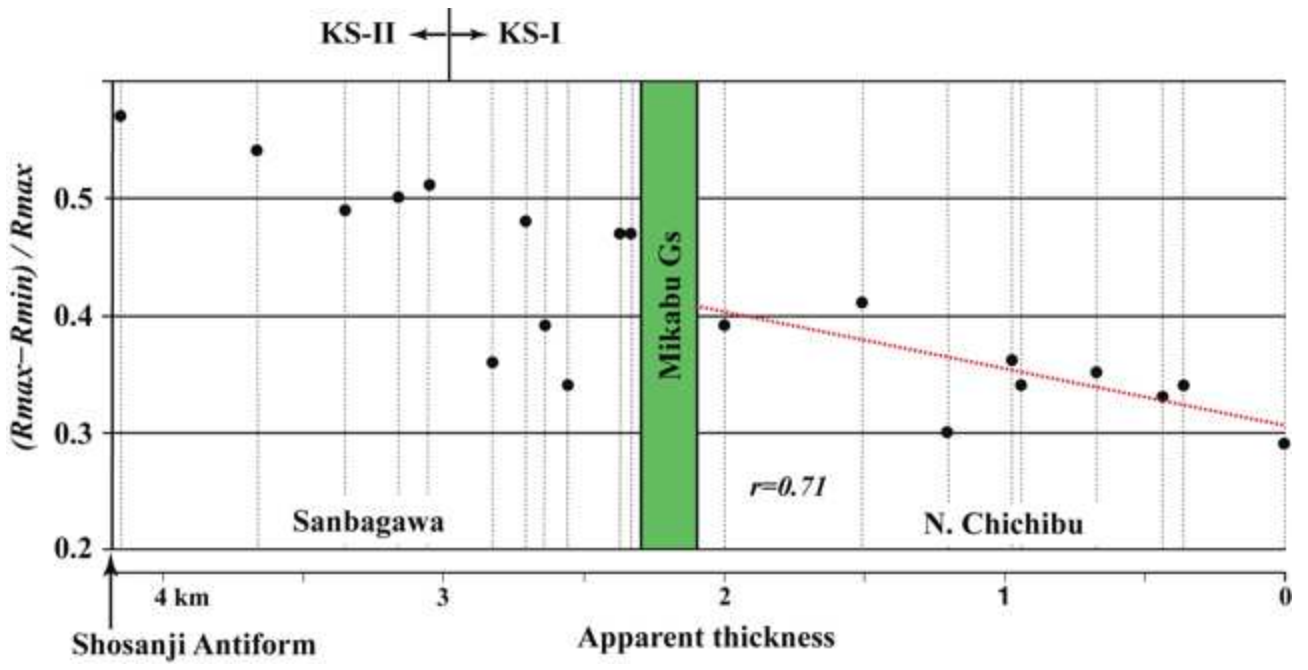
~p'!R ~wíç•Ý§Ç¶ÜqÓé·μ

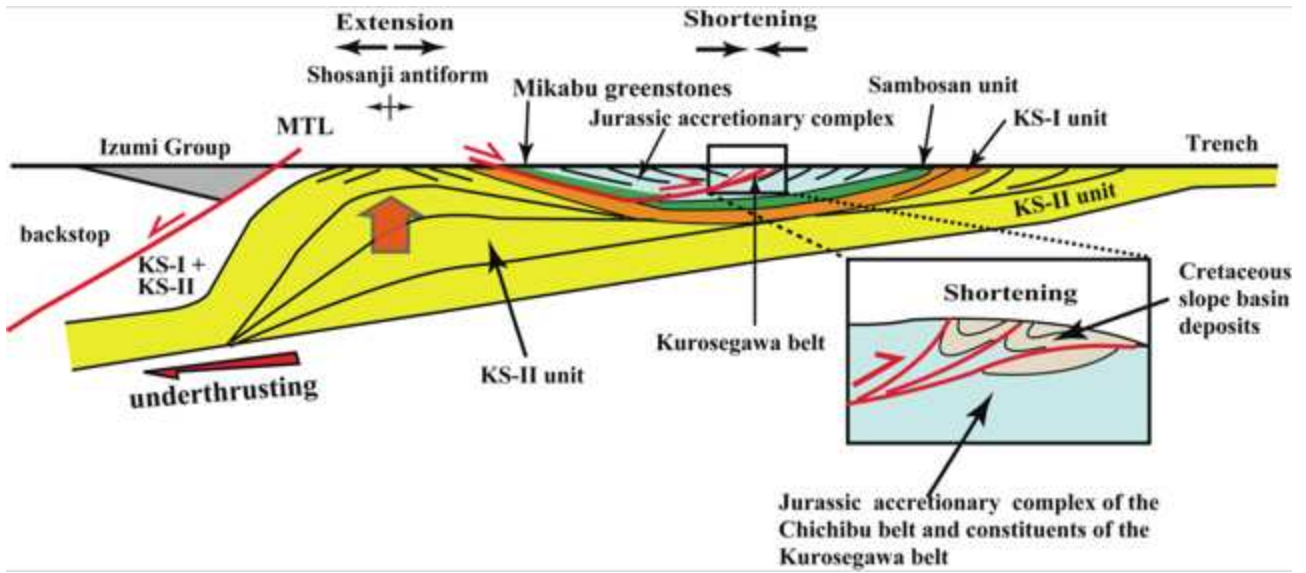


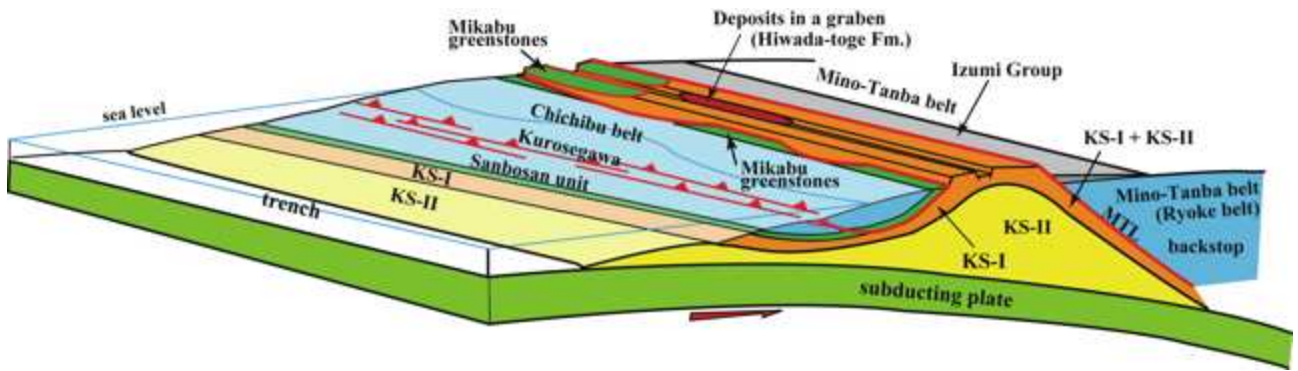
E. Shikoku











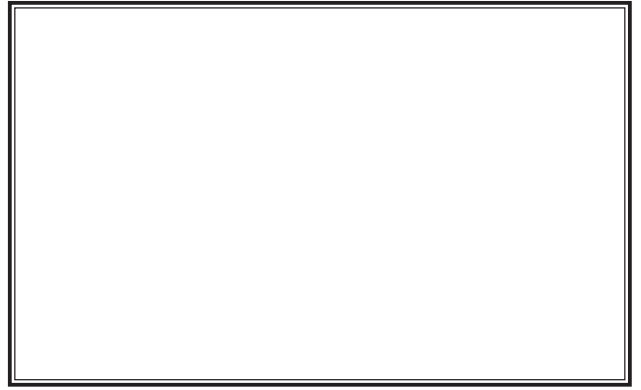
~p'!R "wíç•Ý§Ç¶ÜqÓé·μ

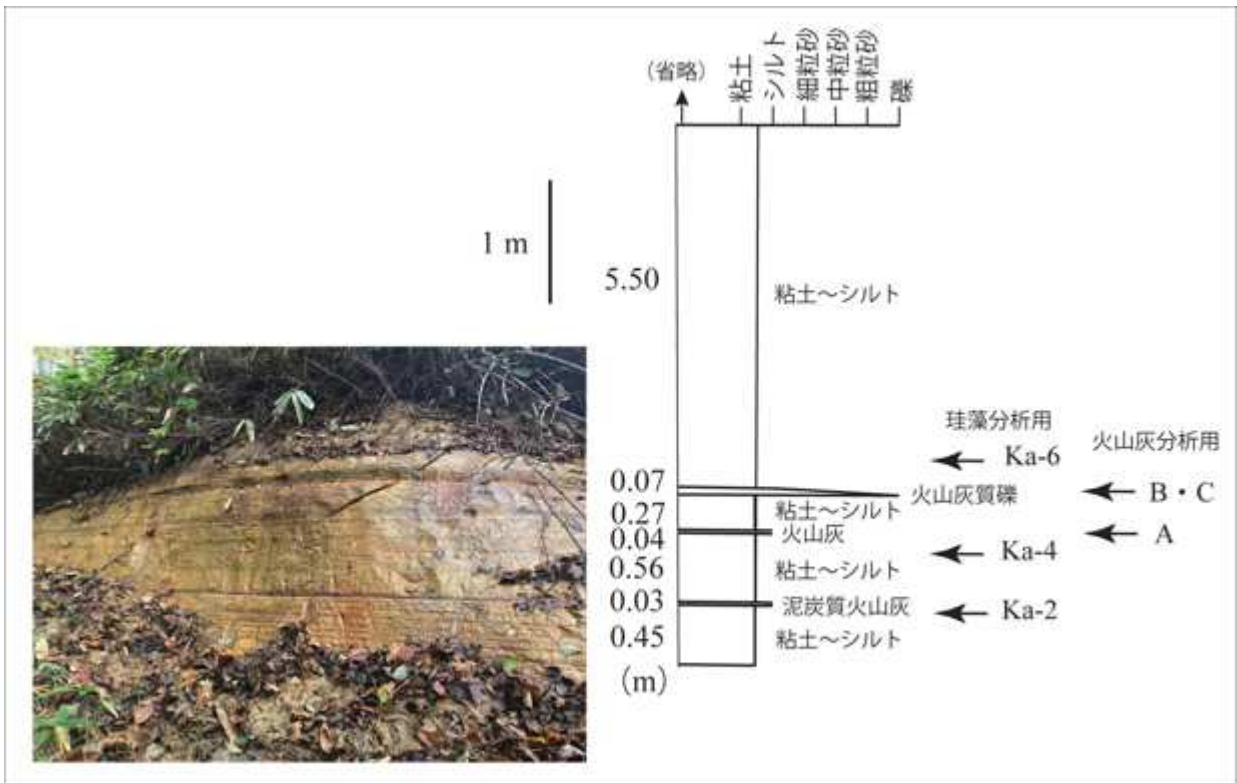
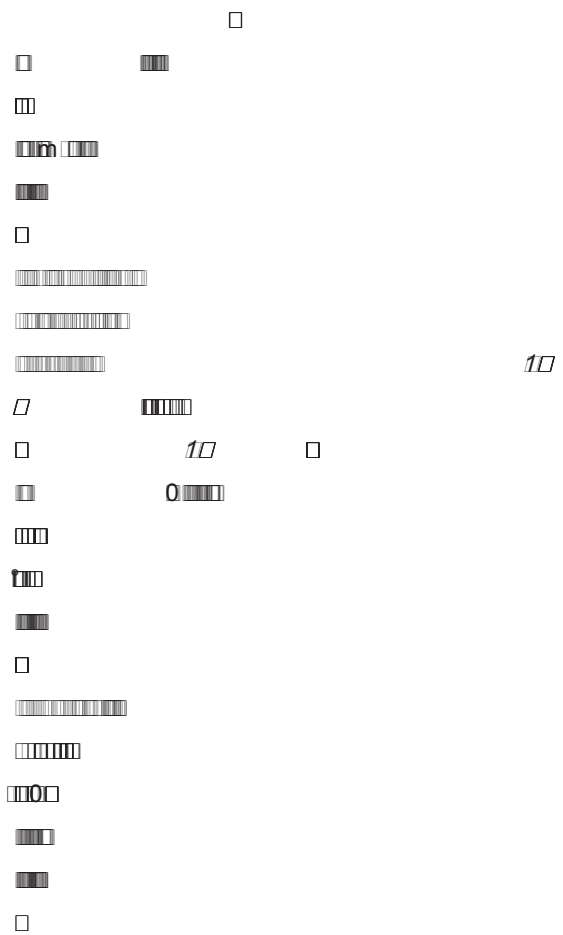
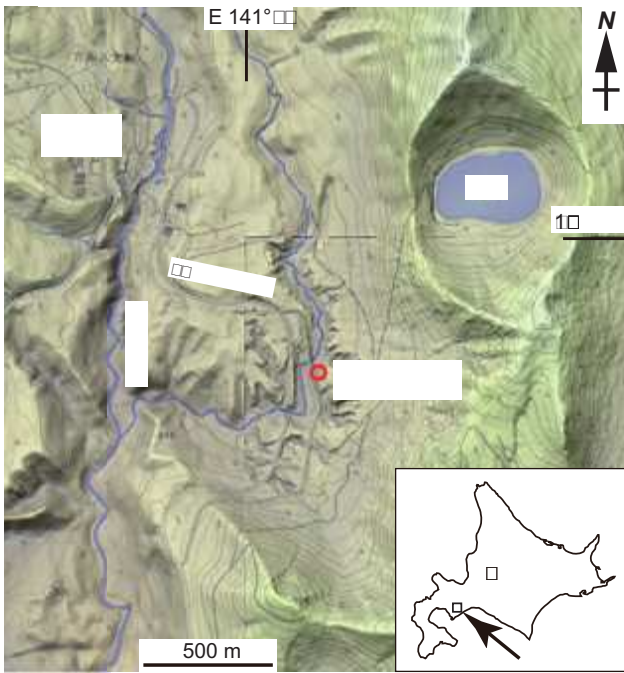
~p'!R "wíç•Ý§Ç¶ÜqÓé·μ

~p!R "wíç•Ý§Ç¶ÜqÓé·μ

Abstract



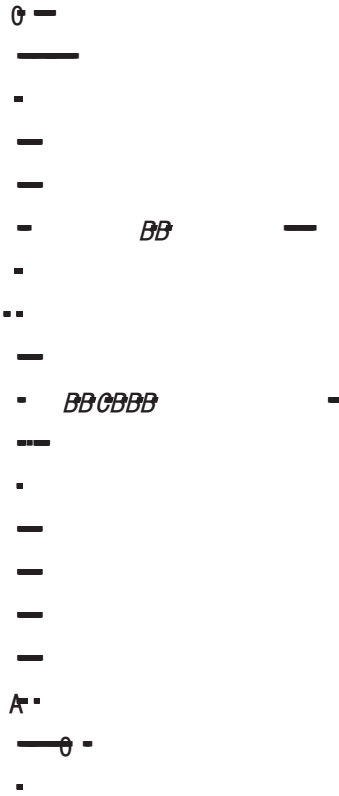




B

Table

Name of species	Name of geologic sample			
	Ecol.	Ka-2	Ka-4	Ka-6
<i>Achnanthes lanceolata</i> Bréb.	F	4	7	3
<i>Caloneis branderii</i> (Hust.) Krammer	F	4	5	1
<i>Cymbella silensiaca</i> Bleisch	F	3	1	
<i>C. tumida</i> (Bréb.) Van Heurek	F	1		
<i>Diatoma vulgare</i> Bory	F			1
<i>Eunotia glacialis</i> Meister	F	7	5	4
<i>E. praerupta</i> Ehr.	F	1	1	1
<i>E. spp.</i>	F	1	5	3
<i>Fragilaria arcus</i> (Ehr.) Cleve	F	6	1	5
<i>F. capucina</i> var. <i>vaucheriae</i> Kütz.	F		2	
<i>F. pinnata</i> Ehr.	F			2
<i>Frustulia rhomboides</i> (Ehr.) De toni	F	5	2	1
<i>F. vulgaris</i> Thwaites	F			4
<i>Gomphonema parvulum</i> (Kütz.) Grun.	F	4		
<i>Navicula bryophila</i> Petersen	F	6	1	2
<i>N. contenta</i> Grun.	F	1	1	
<i>N. pupula</i> Kütz.	F	1		
<i>Nitzschia frustulum</i> (Kütz.) Grun.	F	1	3	1
<i>N. perminuta</i> (Grun.) Peragallo	F		5	2
<i>Pinnularia borealis</i> Ehr.	F	2		1
<i>P. gibba</i> Ehr.	F	12	8	9
<i>P. interrupta</i> W. Smith	F	1		
<i>P. microstauron</i> (Ehr.) Cleve	F			1
<i>P. subcapitata</i> (Ehr.) Greg.	F	30	37	32
<i>P. viridis</i> (Nitzsch.) Ehr.	F	1	3	4
<i>P. spp.</i>	F	6	3	5
<i>Surirella linealis</i> W. Smith	F	2	10	12
<i>S. minuta</i> Bréb.	B-F			6
<i>Synedra ulna</i> (Nitzsch) Ehr.	F	1		
Total valves counted		100	100	100
<input type="checkbox"/>	M	0	0	0
<input type="checkbox"/>	M-B	0	0	0
<input type="checkbox"/>	B	0	0	0
<input type="checkbox"/>	B-F	0	0	6
<input type="checkbox"/>	F	100	100	94
Total		100	100	100
Salinity index		1.00	1.00	1.06



A

A (%) 200

		2		
bw	pm	9.0		45.5
23.5	22.0			

(%)

			0
		0	

B (%) 200

		2		
bw	pm	27.5	1.0	62.0
5.5	4.0			

(%)

			0
50		50	

C (%) 200

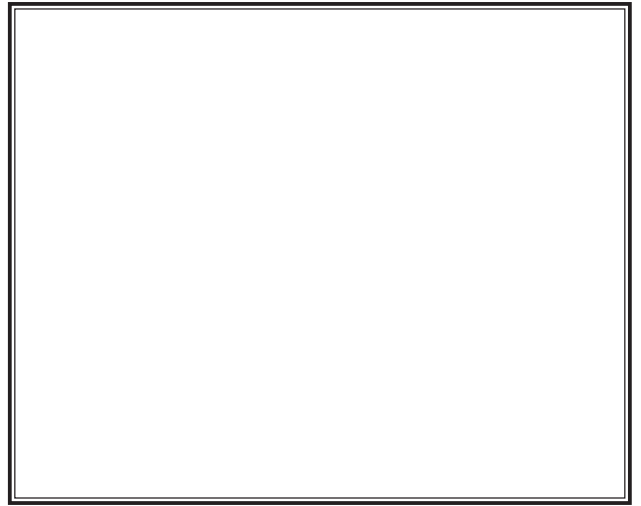
		2		
bw	pm	42.5	1.0	51.0
3.5	2.0			

(%)

			0
100			

Abstract

--



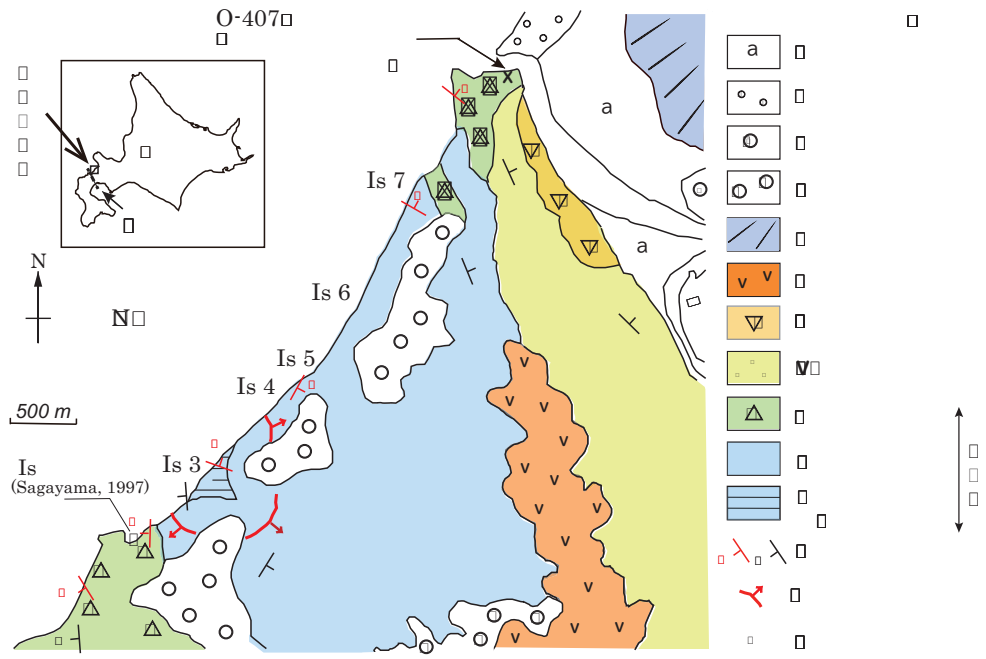
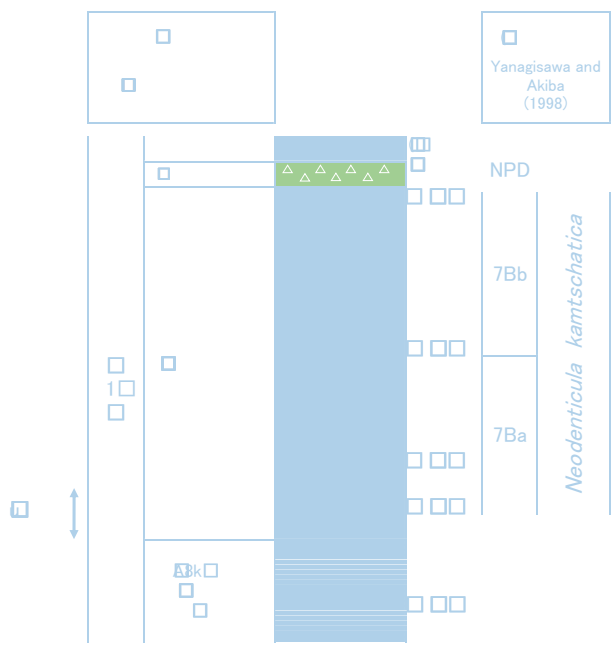


Figure 1
 Map of Is 3 (Sagayama, 1997) and surrounding islands (Is 4, Is 5, Is 6, Is 7).
 NSNNID



0 1 2 3 4 5 6 7 8 9 10

□

TOP DB DP NPB TH BDPB

BNBNB

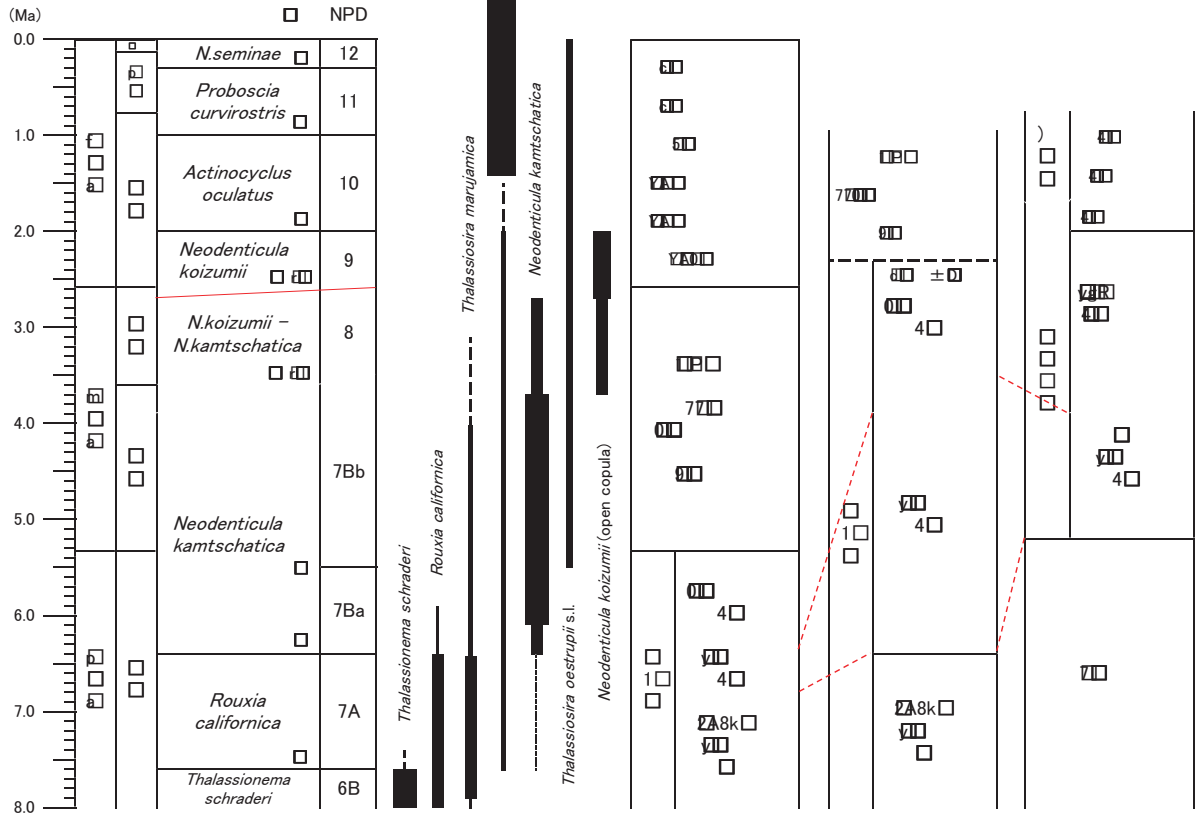
H 95AL

5BCM 11BPGPTTJMTZJMEEGSP 41MTPO 10SPG 11PZB

PSBJPO 7

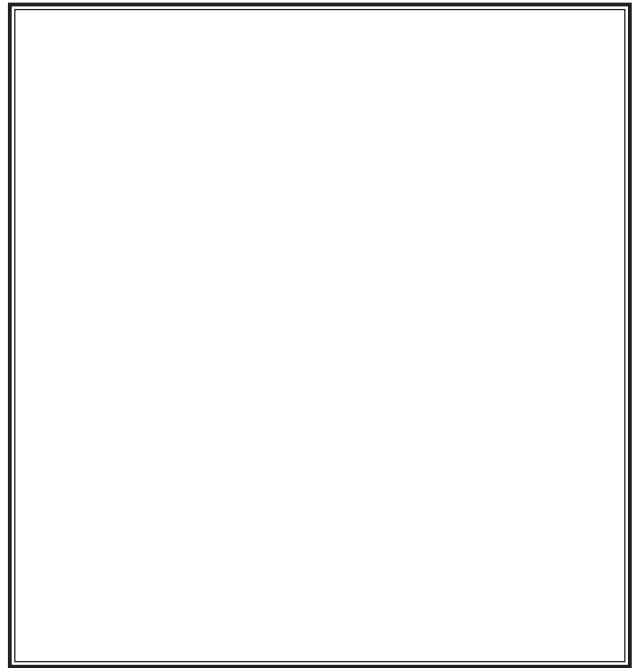
Diatom zones		7Ba		7Bb	
Diatom species	Geologic samples	Is 4	Is 5	Is 6	Is 7
<i>Actinoptychus senarius</i> (Ehr.) Ehr.		1	1		
<i>Amphora</i> sp.				1	
<i>Cocconeis californica</i> Grun.		1	2		
<i>C. clandestina</i> Schmidt				1	
<i>C. costata</i> Greg.		1	4	4	2
<i>C. disculus</i> Schumann		1			
<i>C. scutellum</i> Ehr.		4	1	3	2
<i>C. sp.</i>			1		
<i>Coscinodiscus marginatus</i> Ehr.		93	51	13	3
<i>C. spp.</i>			1		2
<i>Cymatosira debyi</i> Temperè and Brun		1		3	
<i>Delphineis cf. angustata</i> (Patt.) Andrews		2	2		
<i>D. kippae</i> Sancetta				2	1
<i>D. surirella</i> (Ehr.) Andrews				4	2
<i>Denticulopsis hustedtii</i> (Simonsen et Kanaya) Simonsen s.l.				1	
<i>Gramatophora cf. oceanica</i> (Ehr.) Grun.				1	
<i>Melosira sol</i> (Ehr.) Kütz.		1		2	
<i>Neodenticula kamschatica</i> (Zabelina) Akiba et Yanagisawa		12	43	90	156
<i>Nitzschia reinholdii</i> Kanaya ex Schrader			1		
<i>N. sp. 1</i>		1		3	1
<i>Odontella aurita</i> (Lyngbye) Agardh		1			
<i>Paralia sulcata</i> (Ehr.) Cleve		3	2	2	
<i>Rhaphoneis cf. ischaboensis</i> (Grun.) Mertz.		5	2		
<i>Rhizosolenia</i> spp.		2	12	10	
<i>Stephanopyxis</i> spp.		5	1	4	7
<i>Thalassionema nitzschioides</i> H. and M. Peragallo		40	39	28	10
<i>Thalassiosira antiqua</i> (Grun.) Cleve-Euler		1	10		
<i>T. borealis</i> Koizumi		5	4		
<i>T. eccentrica</i> (Ehr.) Cleve		1	1		1
<i>T. hyalina</i> (Grun.) Gran			1		
<i>T. lineata</i> Jousé		1			
<i>T. manifesta</i> Sheshukova-Poretzkaya				1	
<i>T. marujamica</i> Sheshukova-Poretzkaya				7	
<i>T. nidulus</i> (Temperè and Brun) Jousé		1			
<i>T. oestrupii</i> (Ostenfeld) Porshkina-Labrenko s.l.				3	1
<i>T. spp.</i>		8	10	8	2
<i>Thalassiothrix frauenfeldii</i> Grun.		4	8	9	7
<i>T. robusta</i> (Schrader) Akiba		5	3	1	2
Total number of valves counted		200	200	200	200

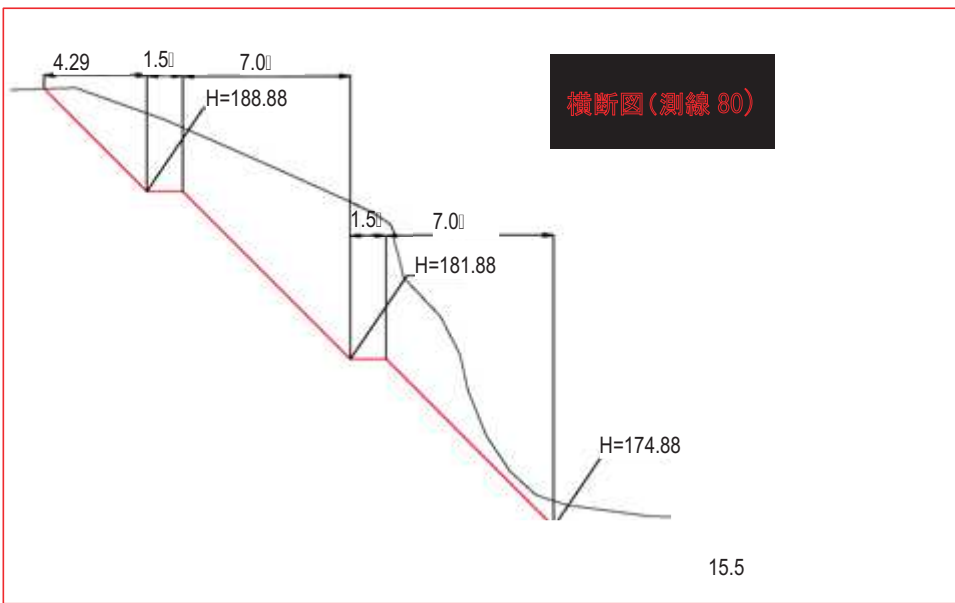
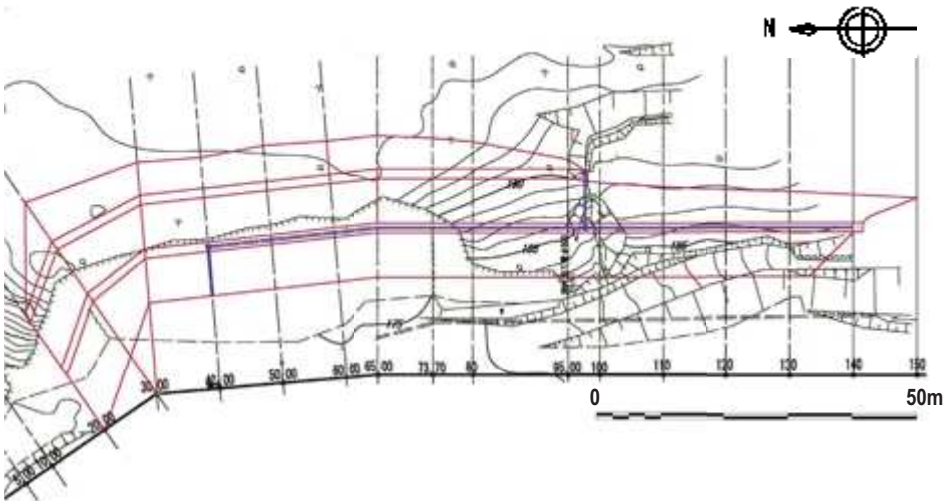
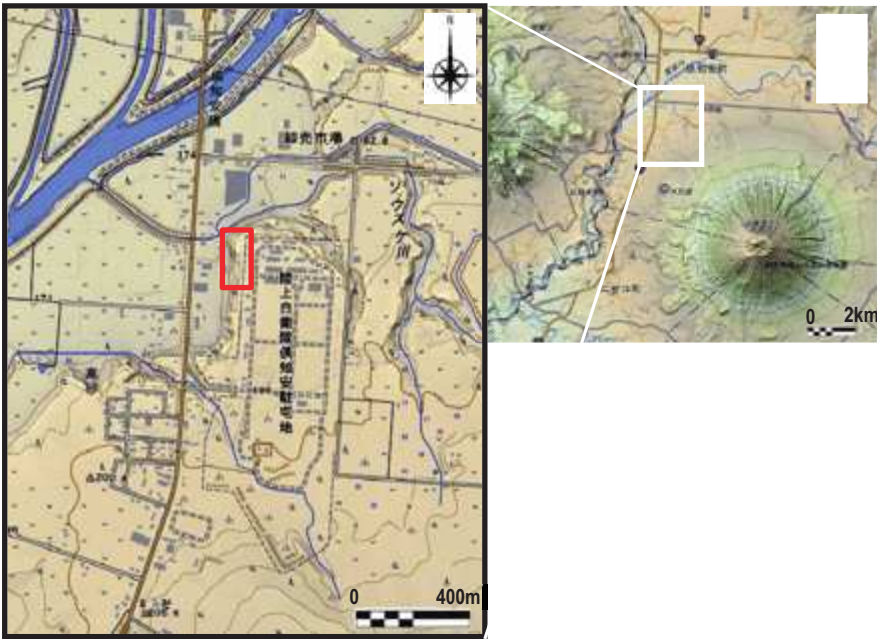
□ Yanagisawa and Akiba (1998)

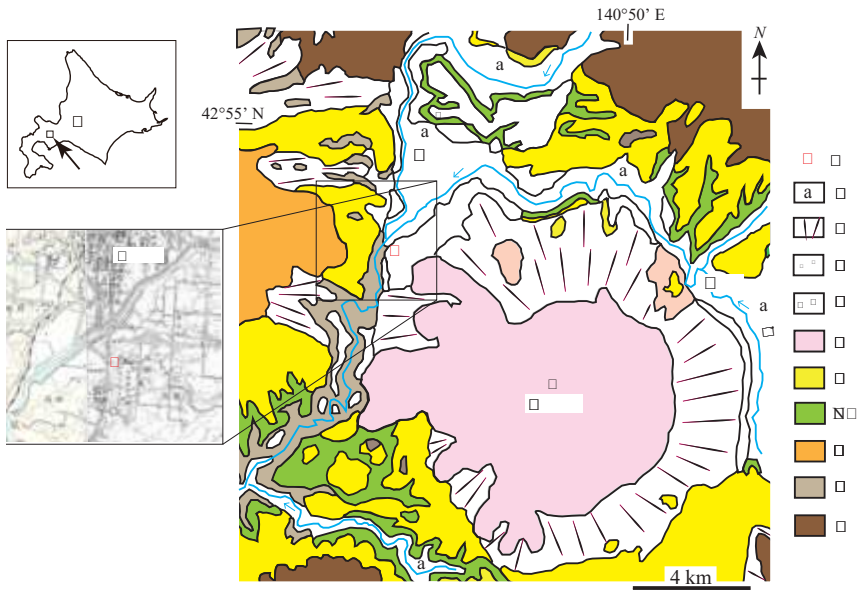


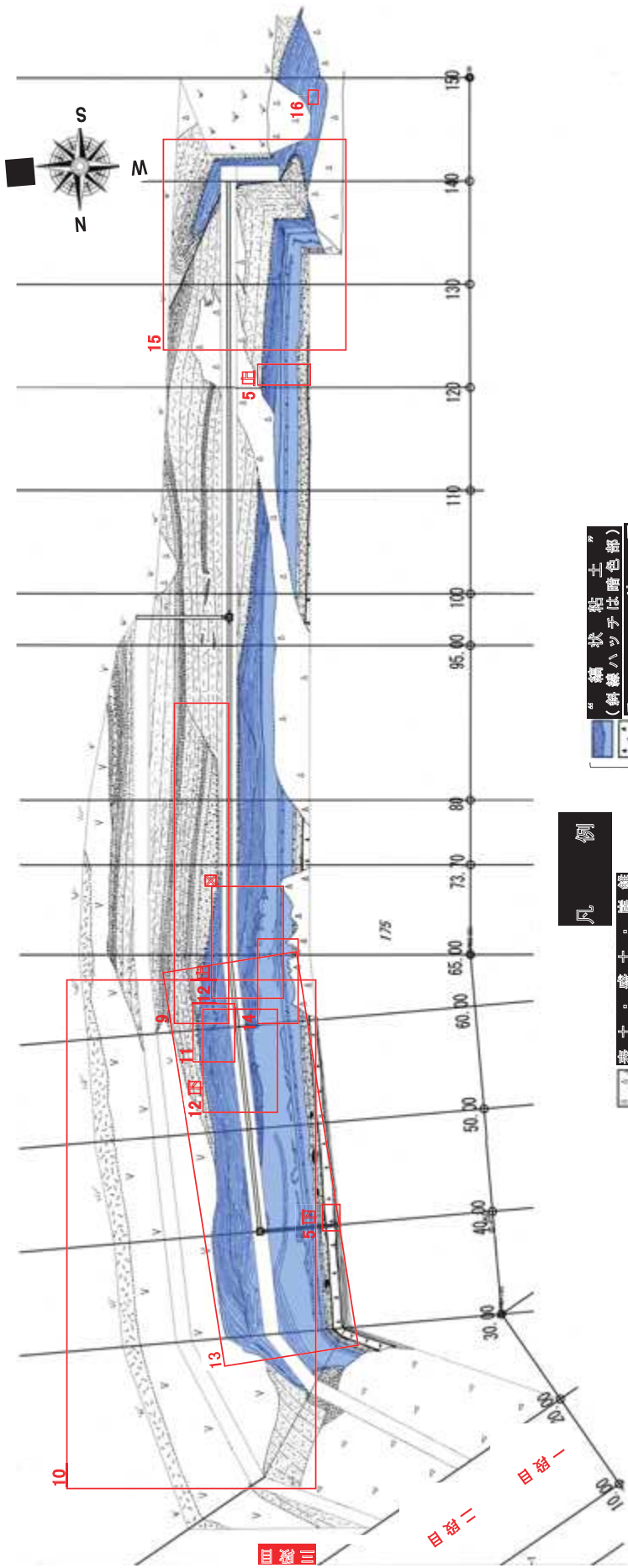
□

Abstract







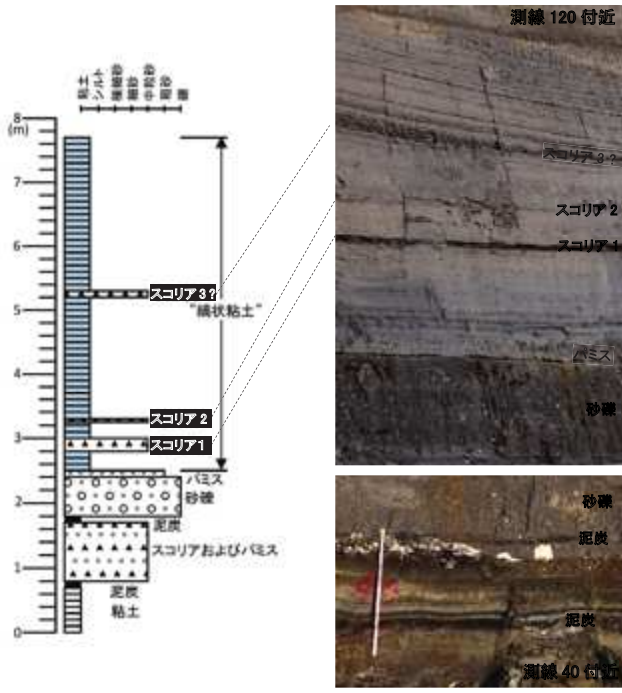


凡例

	表土・盛土・盛盤
	岩屑なだれ堆積物
	成層した凝灰質砂礫
	砂
	シル
	写真位置(数字は図番)

	“綿状粘土” (綿線ハツチは暗色部)
	ス コ リ ア
	砂礫 (パミス多含)
	砂
	泥
	粘 土
	境界
	質地は褐色化の下段) 本文中で化学組成を 検討した礫石採取地

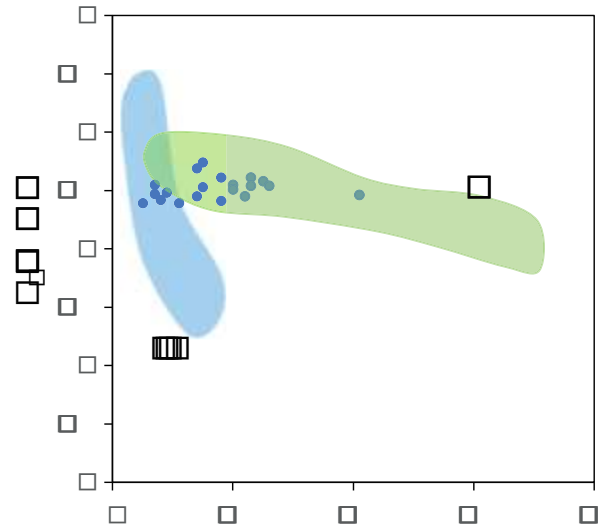




□□□□



□□□□



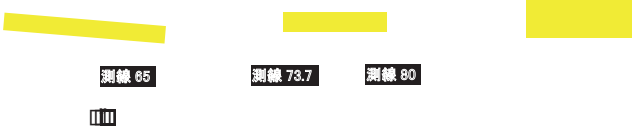
□□□□

□□□□

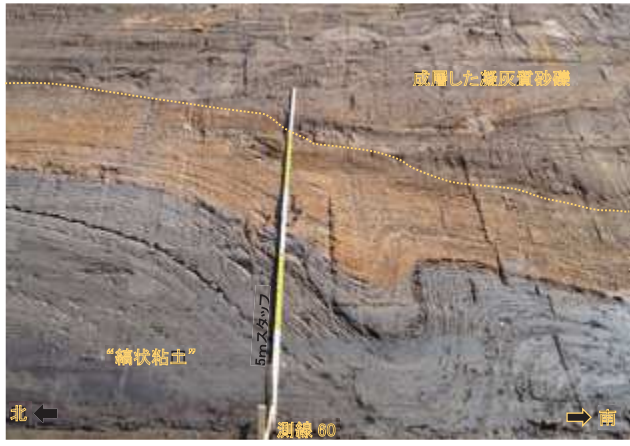
□□

□□□□

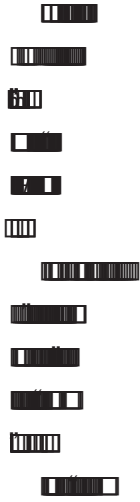
□□

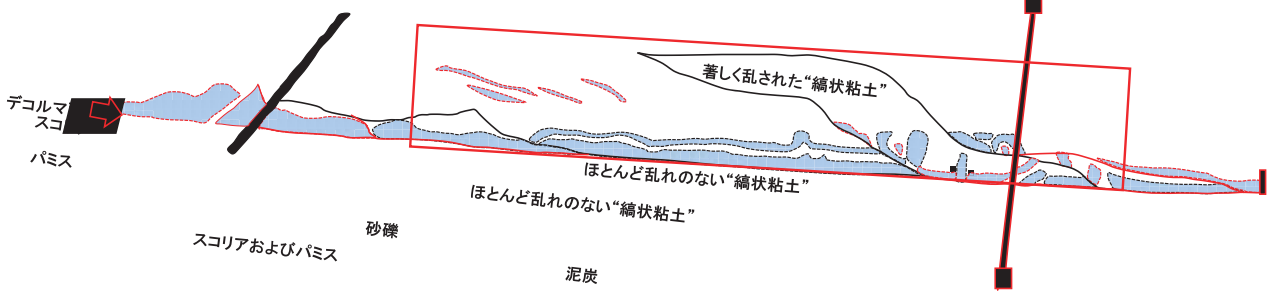
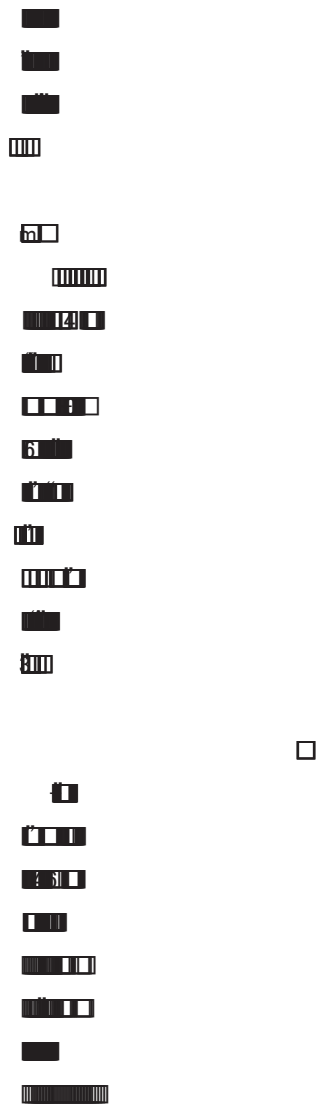
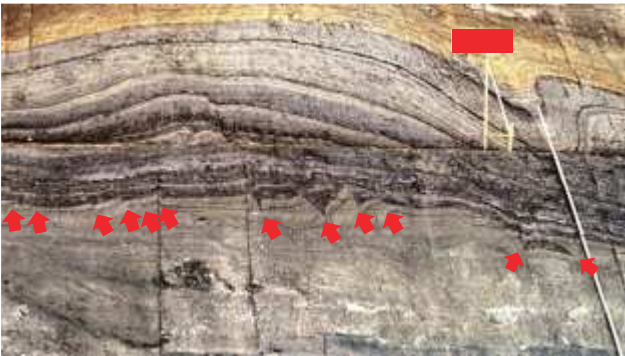
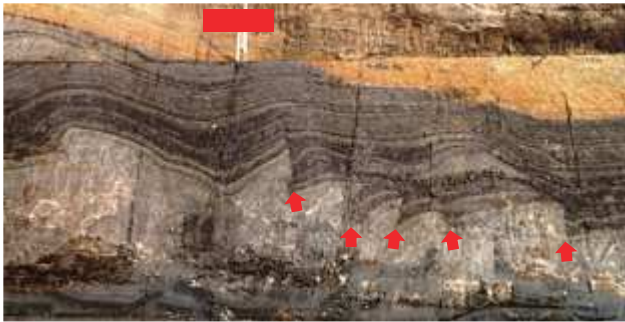


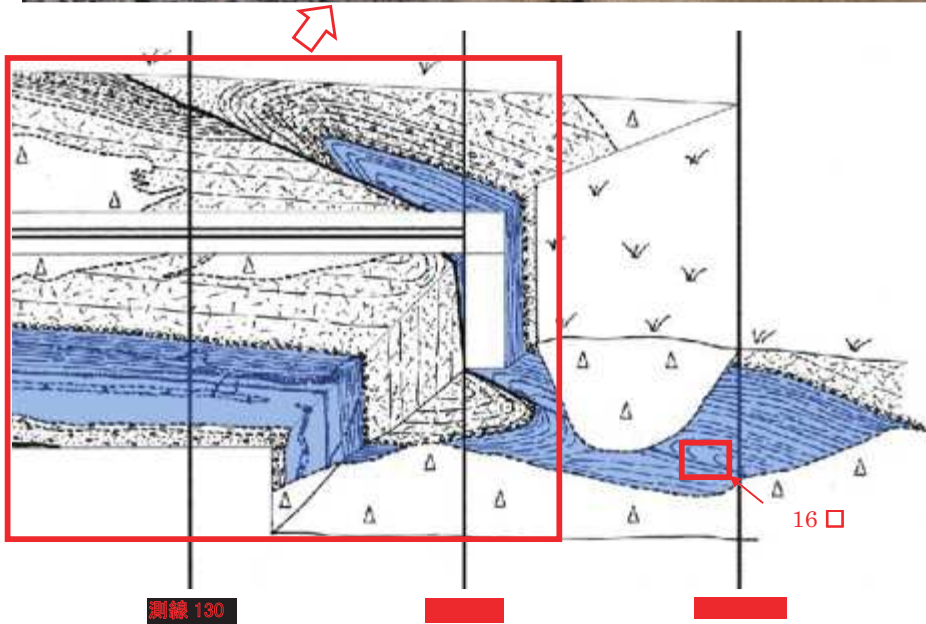
0.5m

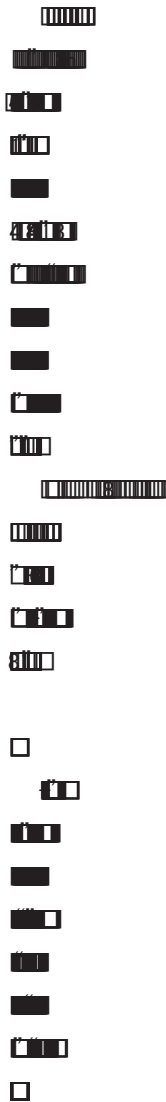
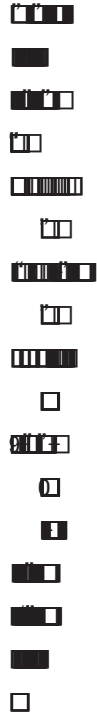
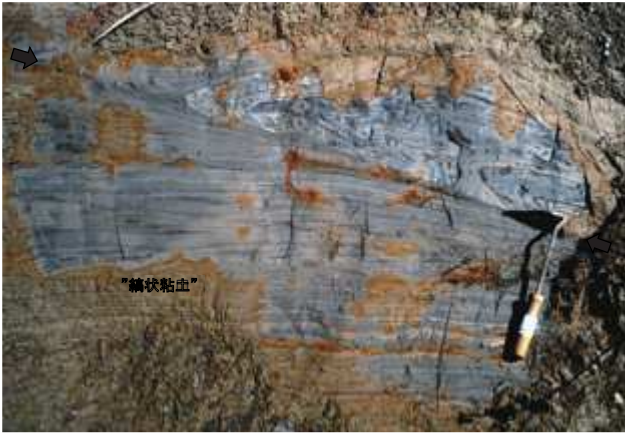


0.5m









а іу |у„Т

апа

апа

апа

апа

апа

апа

апа

апа

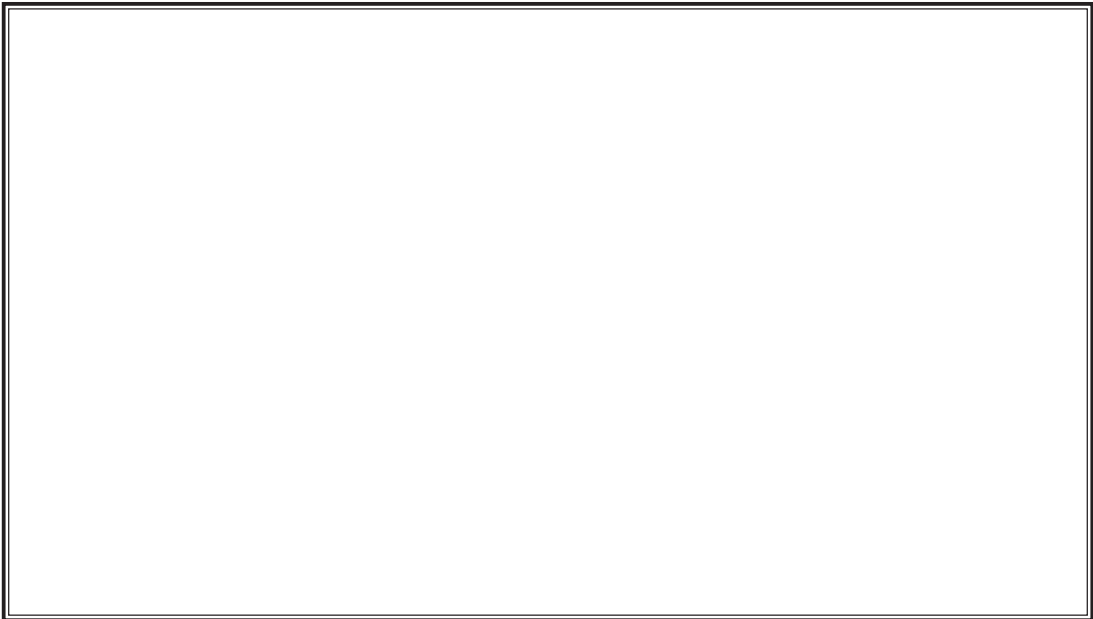
апа

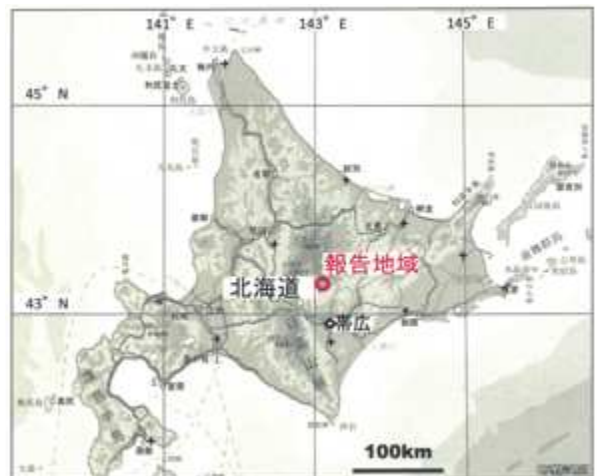
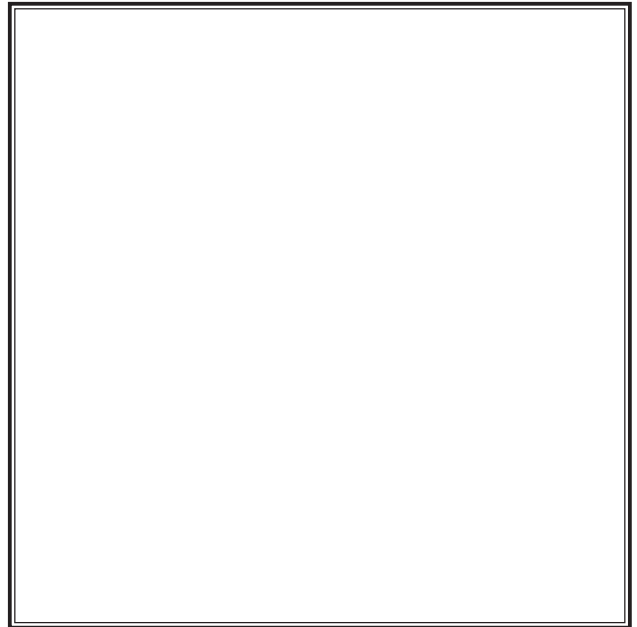
апа

апа

апа

Abstract

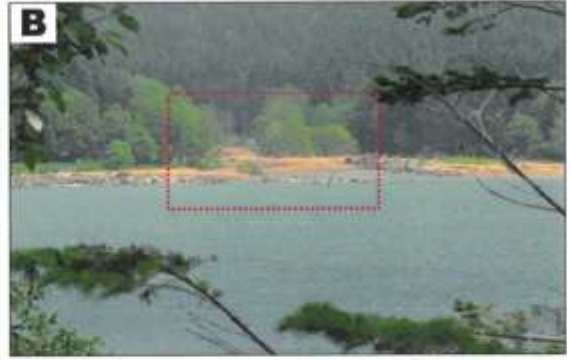
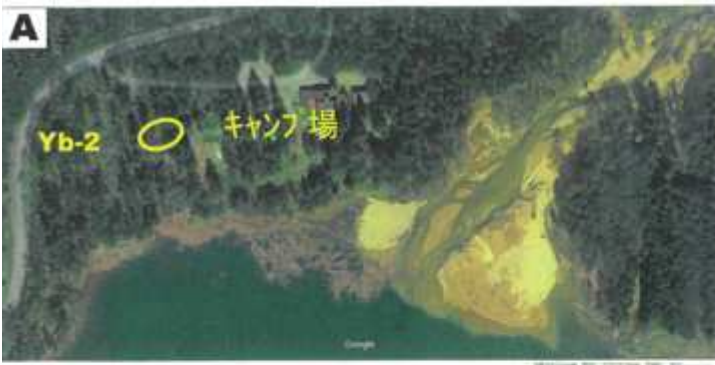


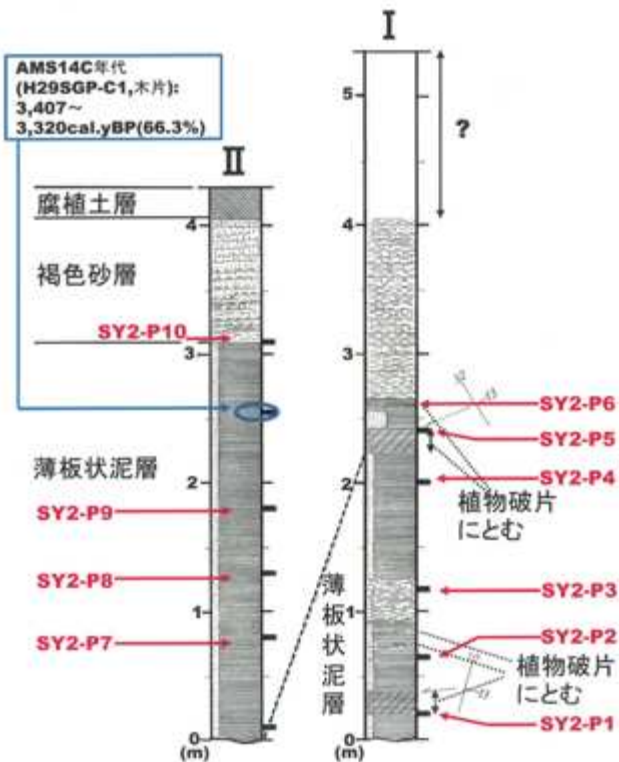
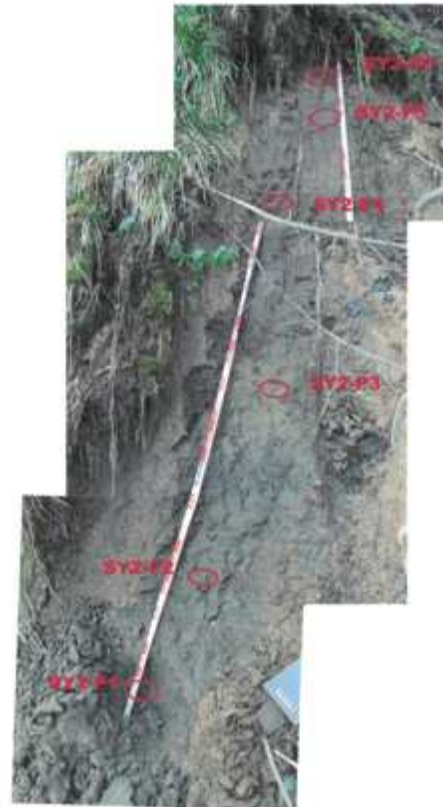


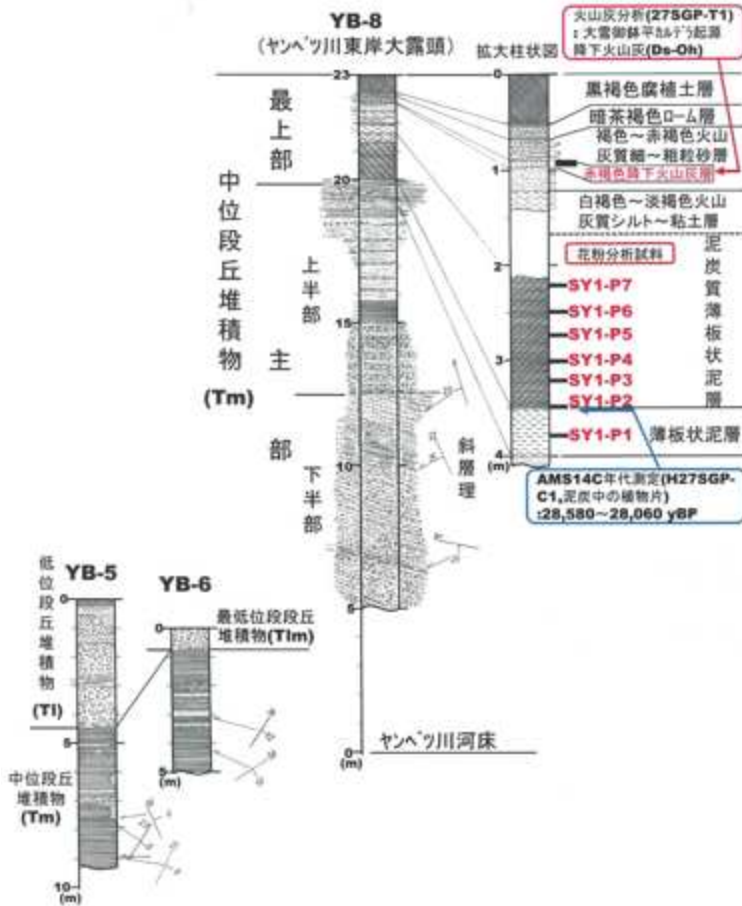
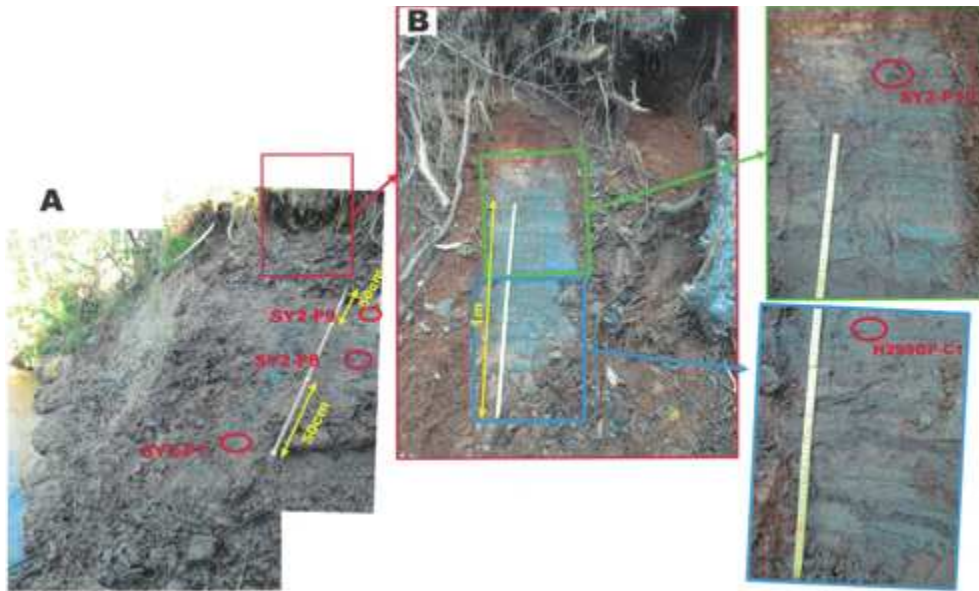
,y' \$ ~ G by k

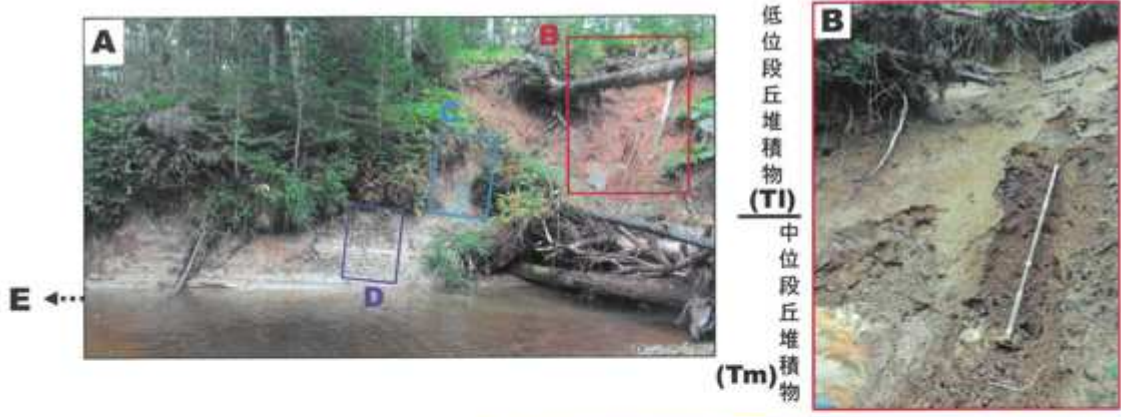


,y' \$ ~ G by k

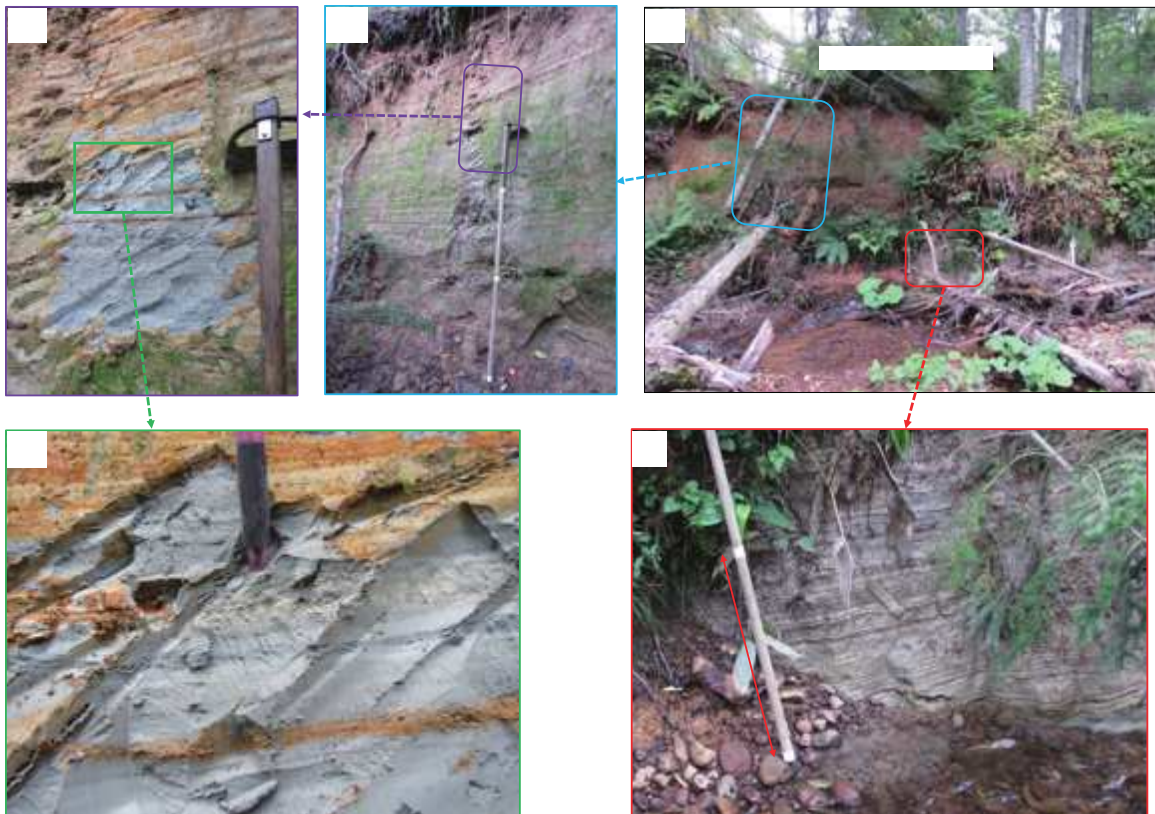


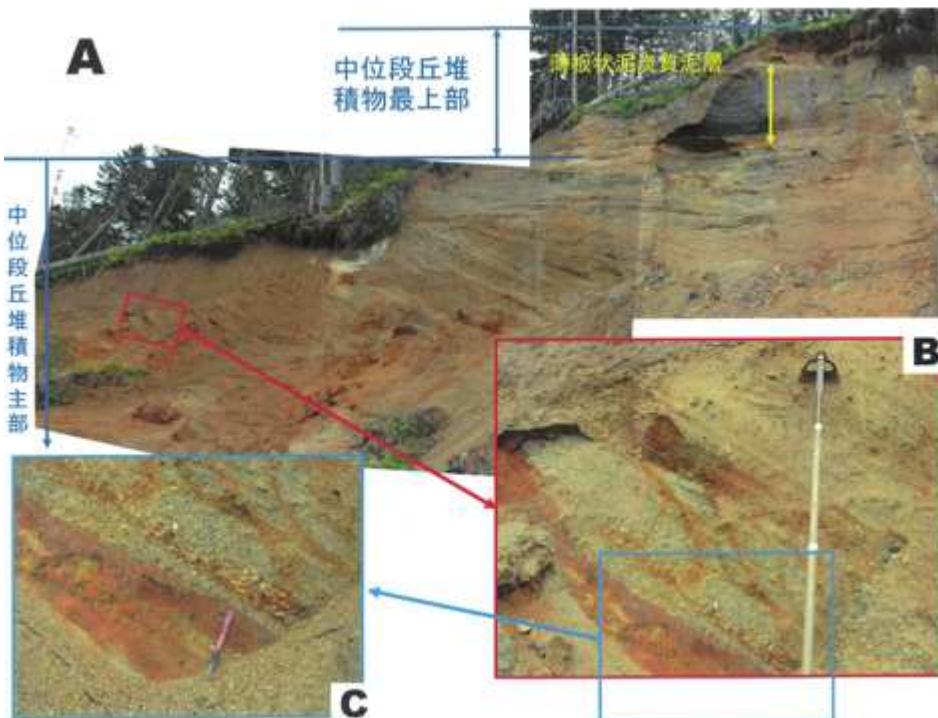


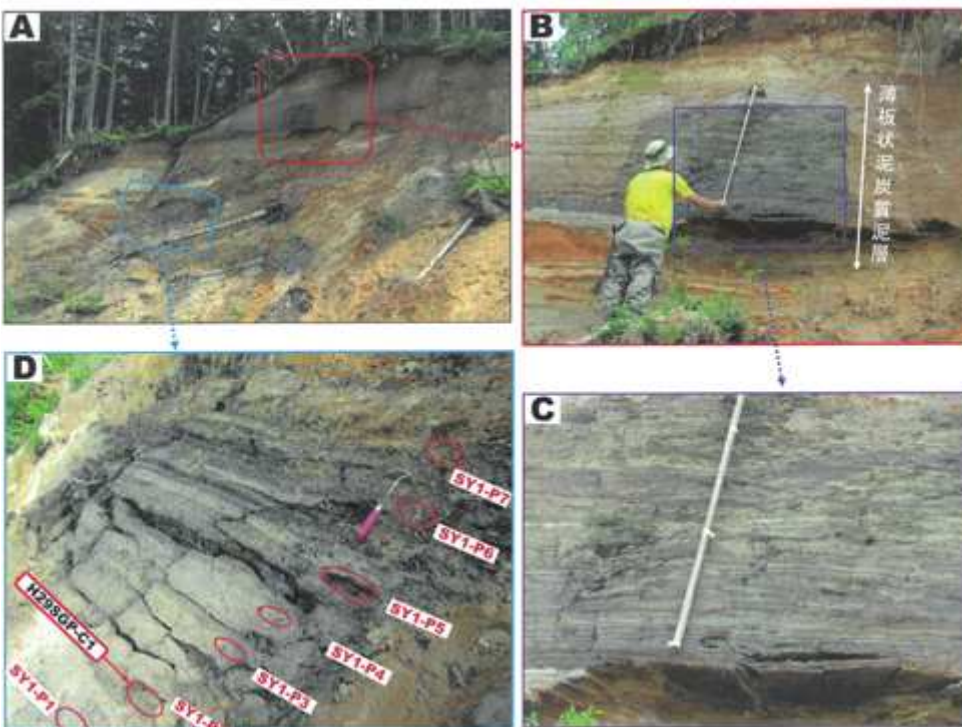


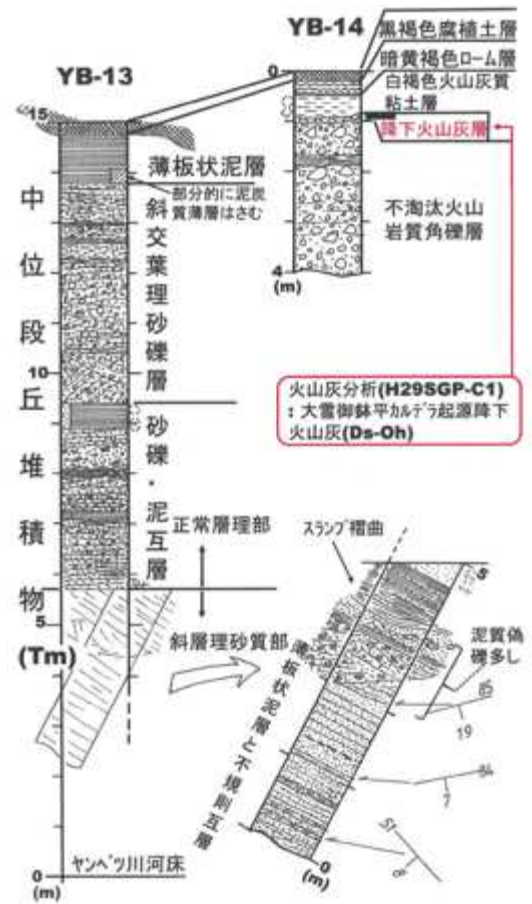
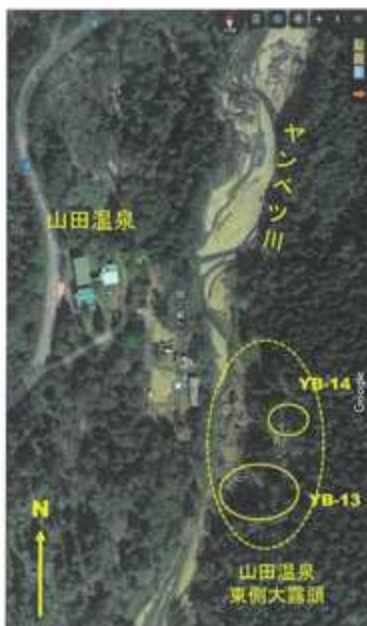


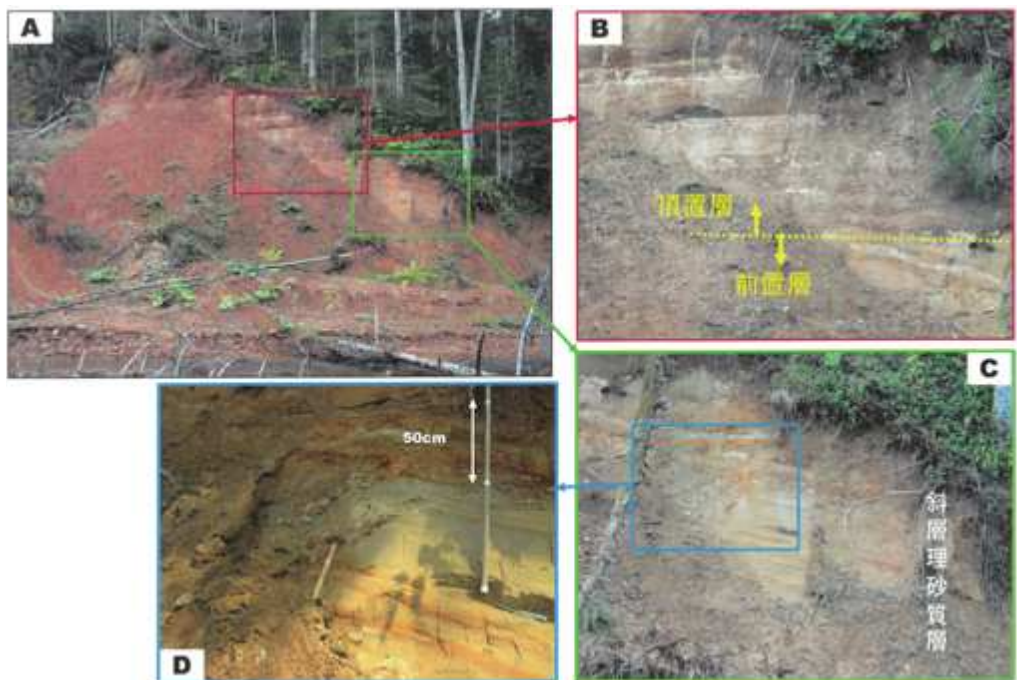
スランプ褶曲

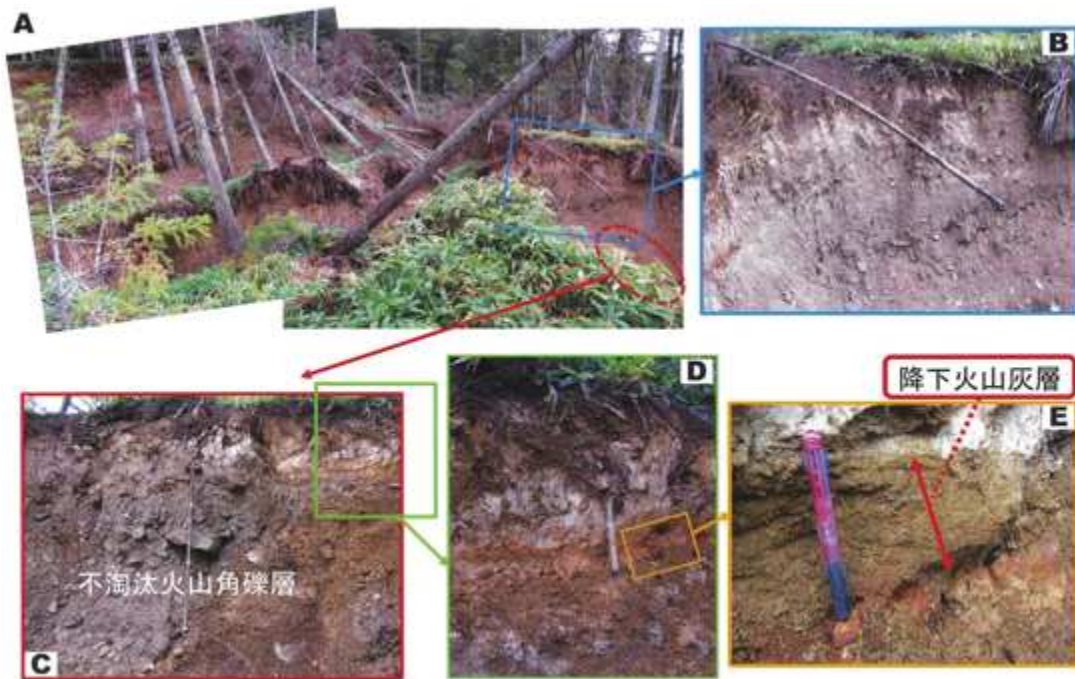
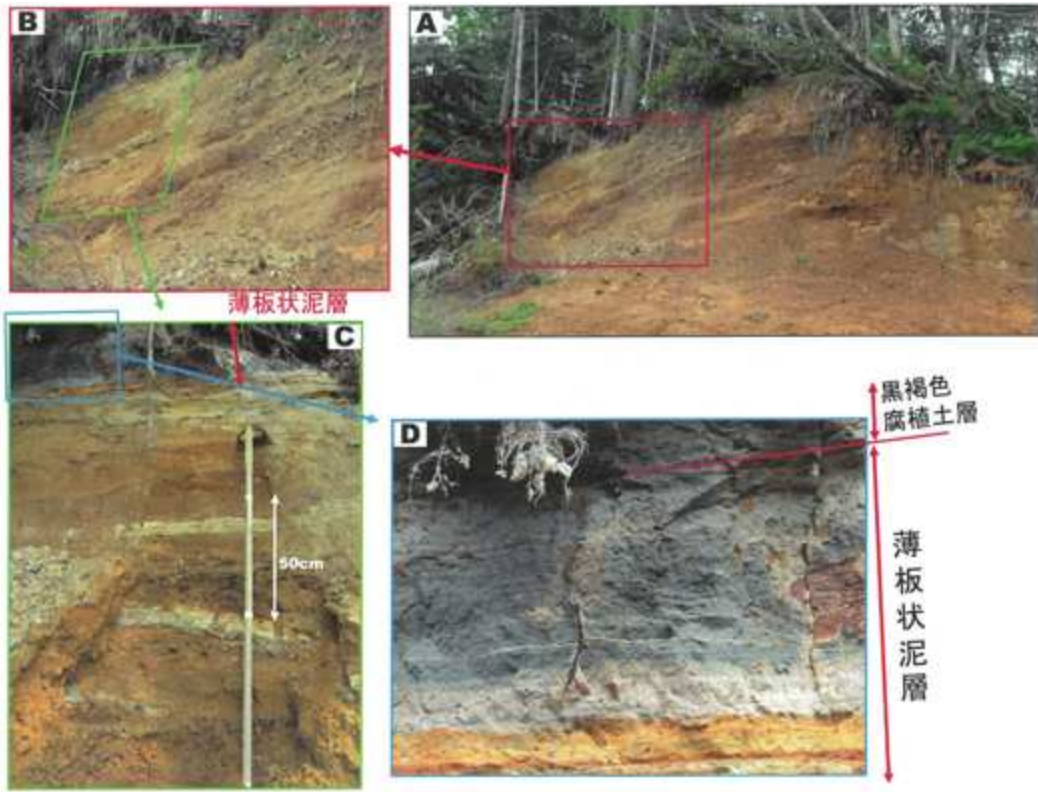


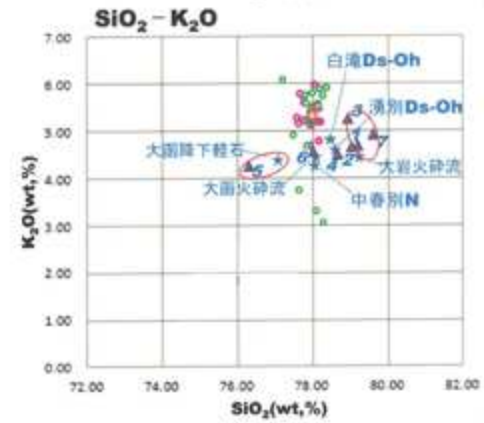
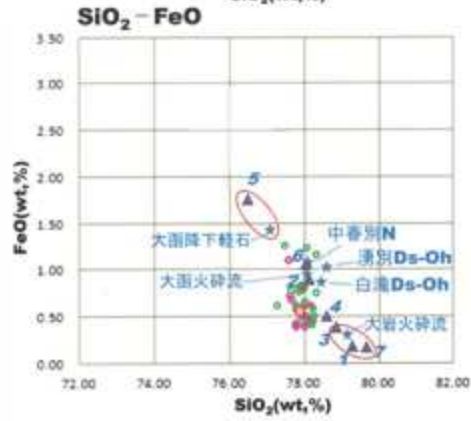
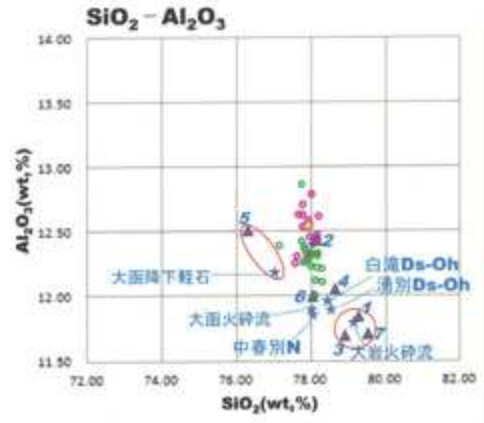
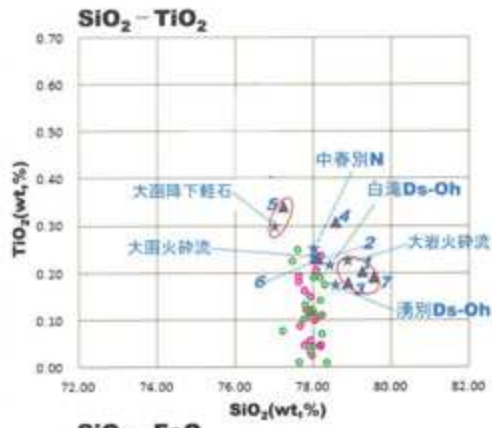












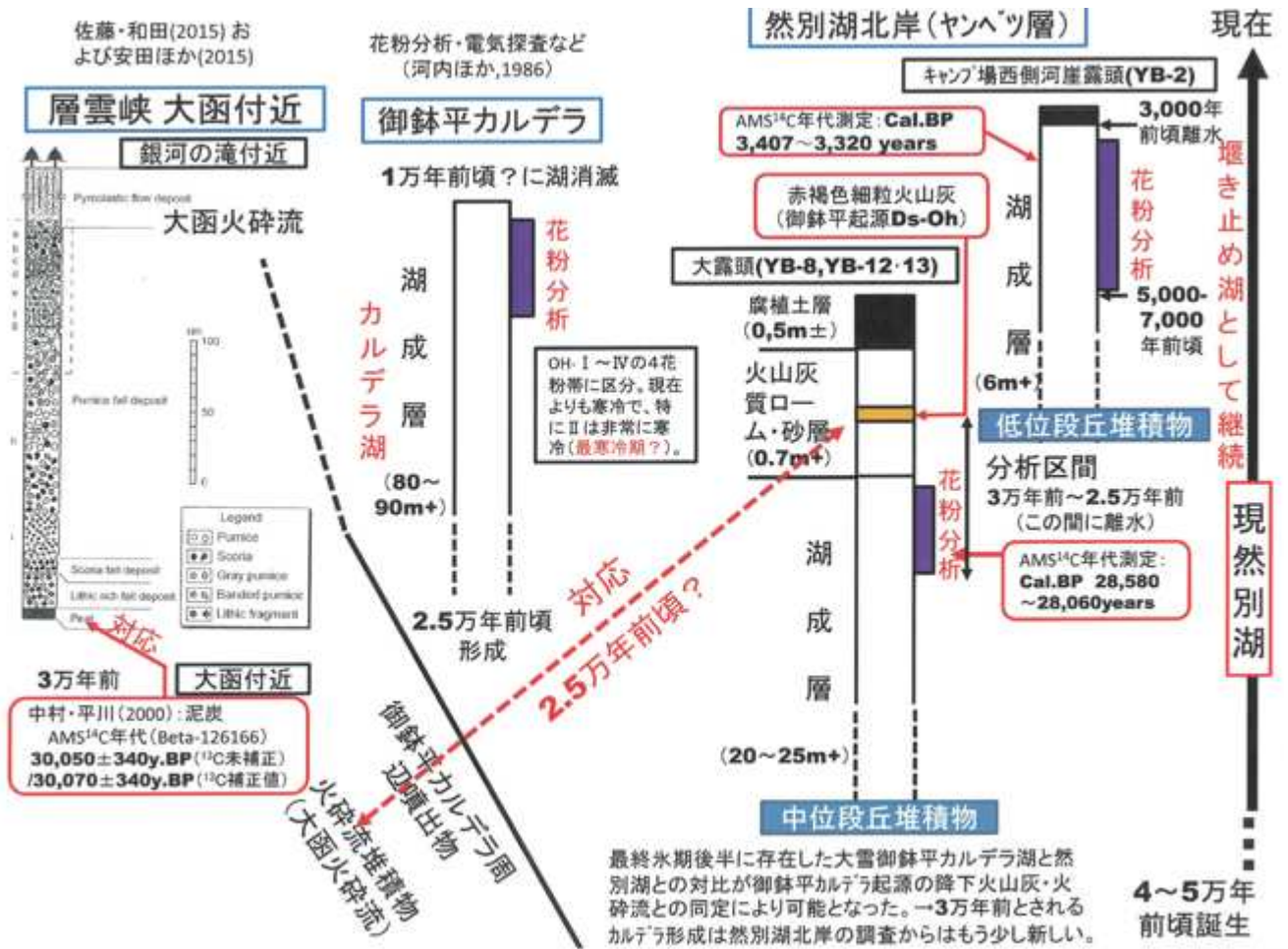
● H27SGP-T1 (下:平均値) ○ H29SGP-T1 (下:平均値)

* 和田ほか(2007)および青木ほか(2006)掲載の御鉢平カルデラ関連火山ガラス分析値

▲ 佐藤ほか(2015)掲載の御鉢平カルデラ関連火山ガラス分析値(オーブ)

,y' \$ ~ G by k

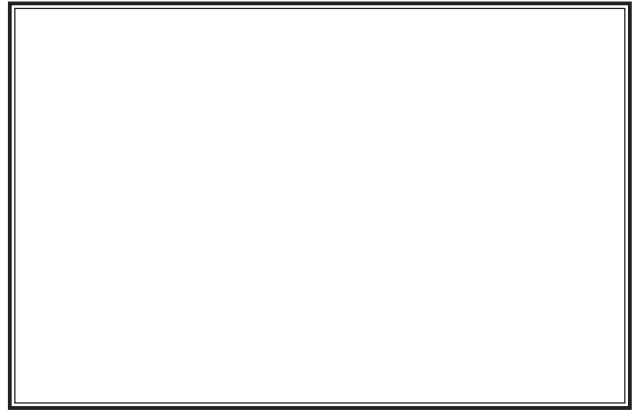
μ „z w„^a/uú



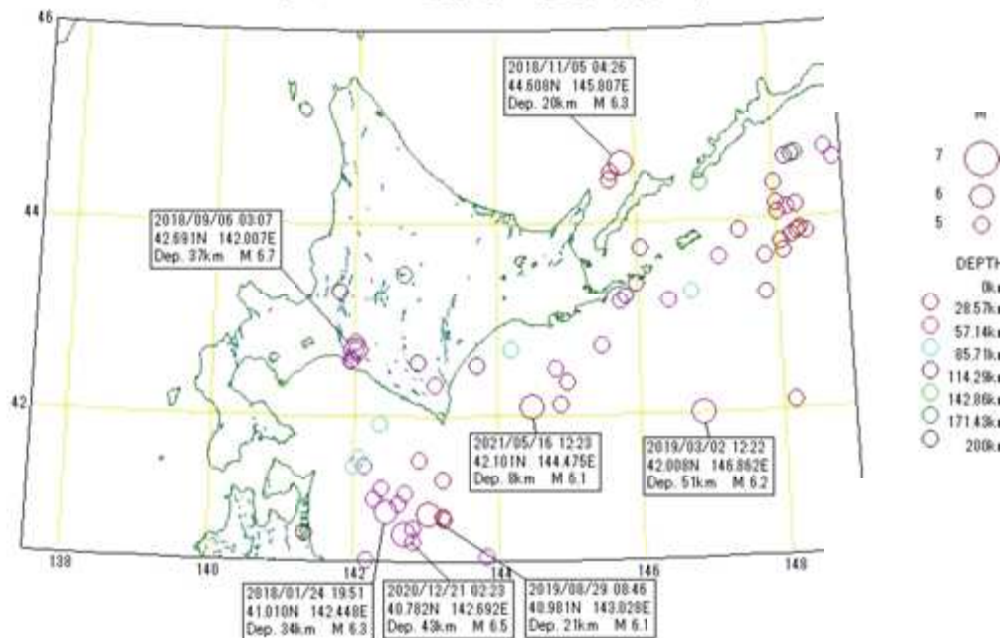
μ „z w„^a/uú

Abstract





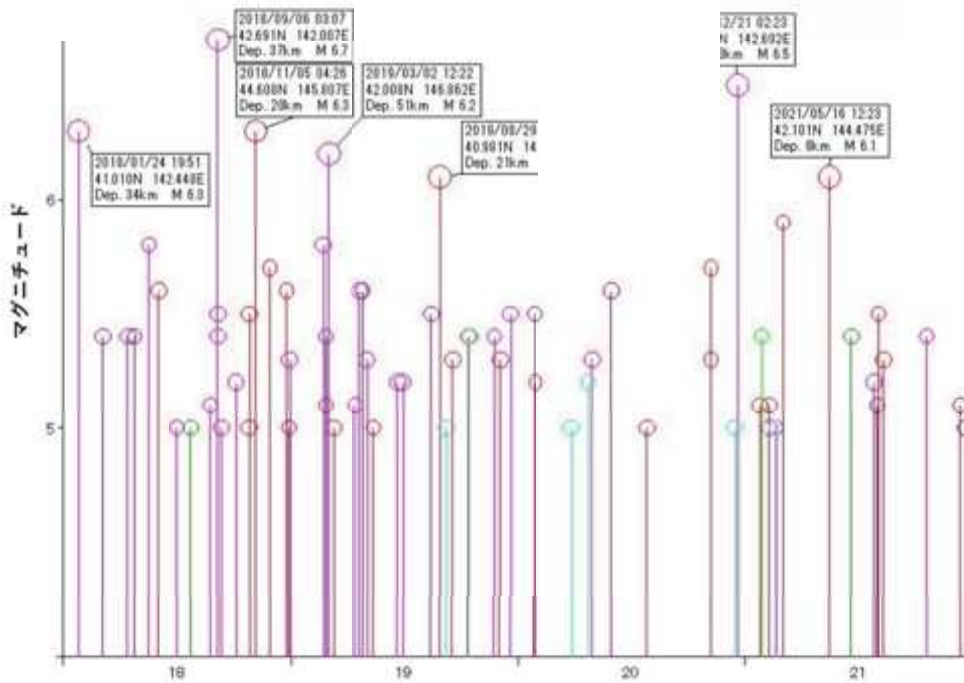
M5以上の地震の震央分布



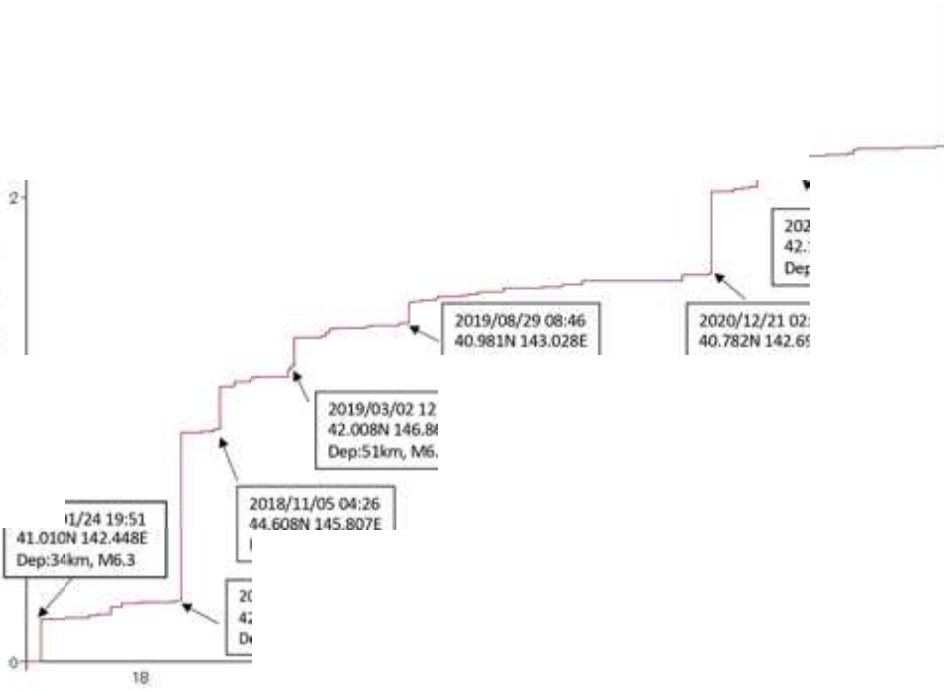
地震

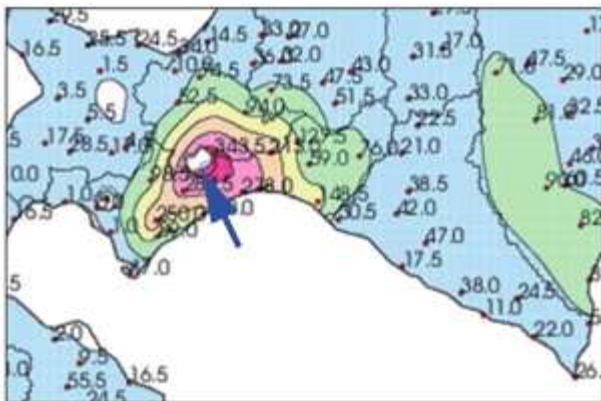
列

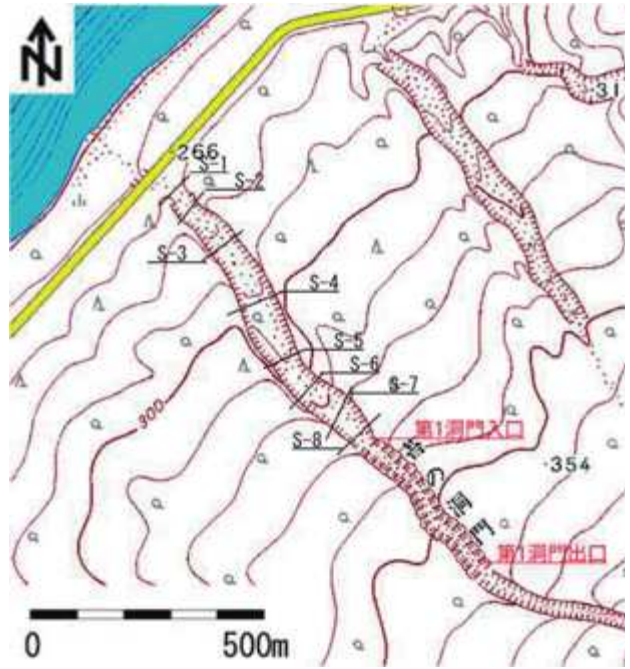
1 -- 2021/12/31 23:59 :M



震波エネルギー (×)

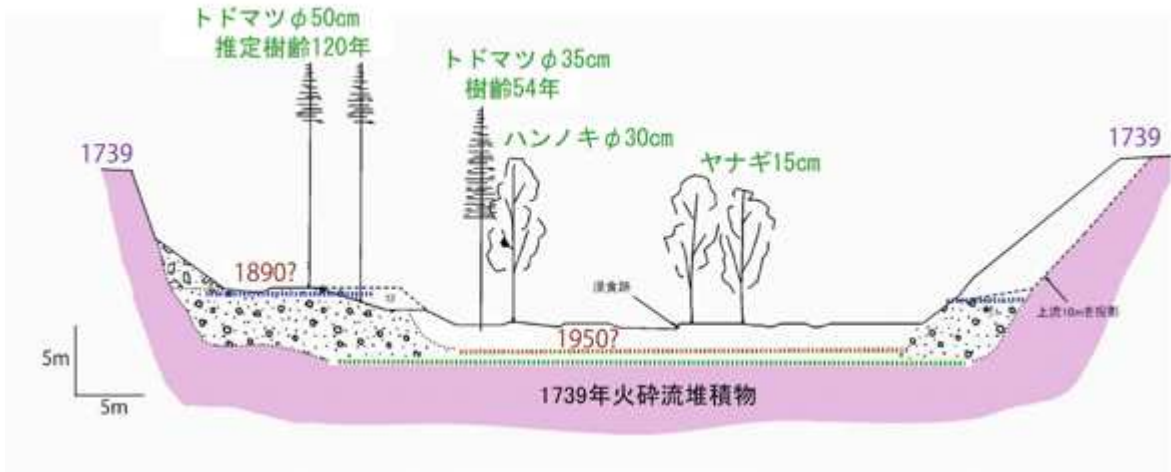


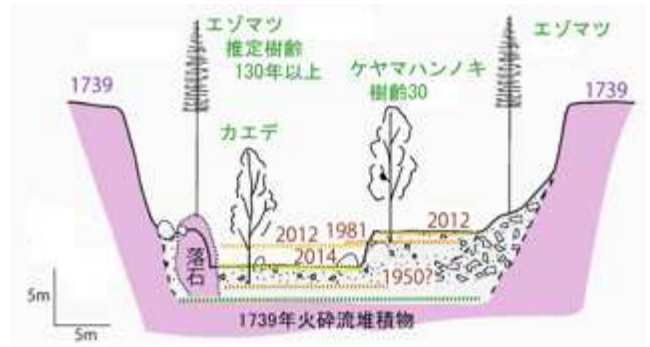












§ G „Æ ® = w Ž ó - w Ń + ™

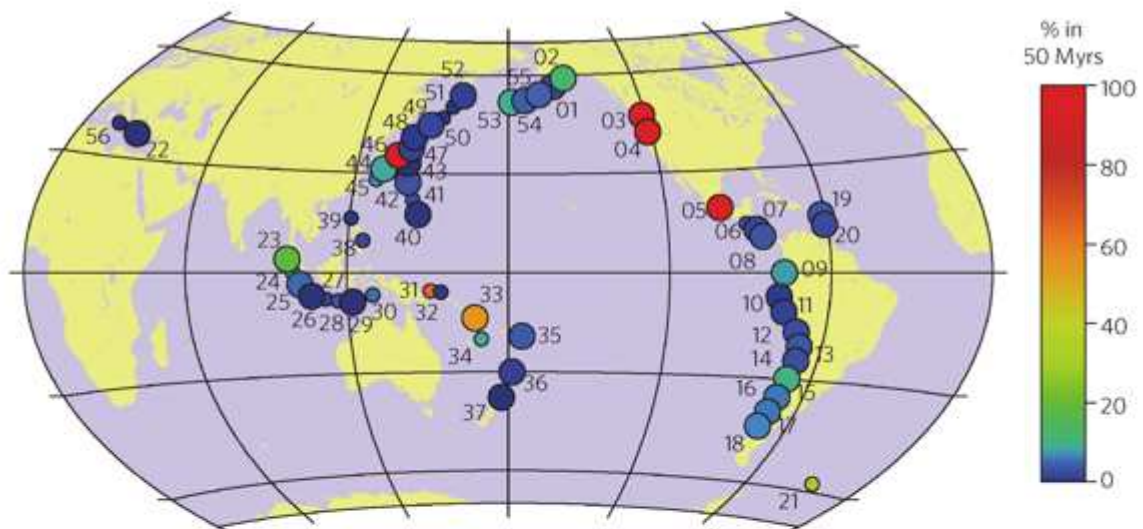


Figure 3 | Predicted per cent hydration of mantle wedges worldwide produced over last 50 Myrs. Predictions from thermal models with decoupling to 80 km and vertical water transport (Supplementary Table 2); models are steady state except where noted in Supplementary Discussion 4. The colours denote hydration, whereas larger circles show arcs with well-constrained geometry (uncertainty in forearc crustal thickness < 10 km and uncertainty in depth to slab below volcanic front³⁸ < 20 km). The numbers code to subduction zones listed in Supplementary Tables 1 and 2, the following of which are discussed in the main text: 1, Alaska Peninsula; 4, Cascadia; 5, Mexico; 31, New Britain; 33, North Vanuatu; 46, Nankai; 48, North Honshu.

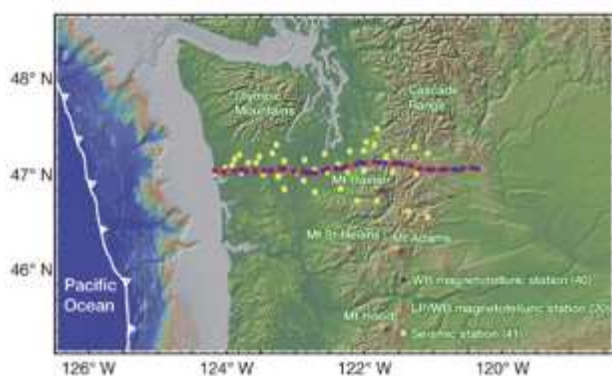


Figure 1 | Map showing station locations for the CAFE seismic and magnetotelluric stations (wideband and long-period) across central Washington state, USA. The numbers in parentheses indicate the number of stations for each category. WB, wideband; LP, long-period.

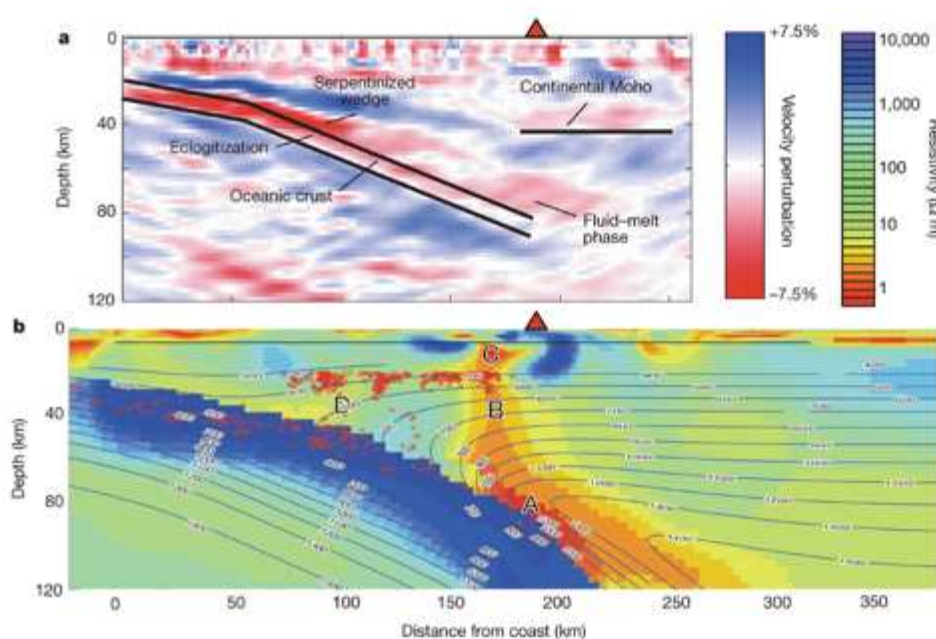


Figure 2 | Primary seismic (a) and magnetotelluric (b) models. Panel b includes both a thermal profile (contours, labelled in degrees Celsius) and earthquake hypocentre locations (red circles) within 20 km of our profile line²³. Fluid released from the subducting slab enters the mantle wedge at A. Melt initiated at or very near the interface is transported upward by buoyancy and dragged down. The fluid/melt phase rises through the mantle wedge (B) until it reaches the crust, joining fluids released from shallower reactions (D). The combined fluid/melt continues to rise until reaching a reservoir (C) in the crust. Mount Rainier is shown as a red triangle.

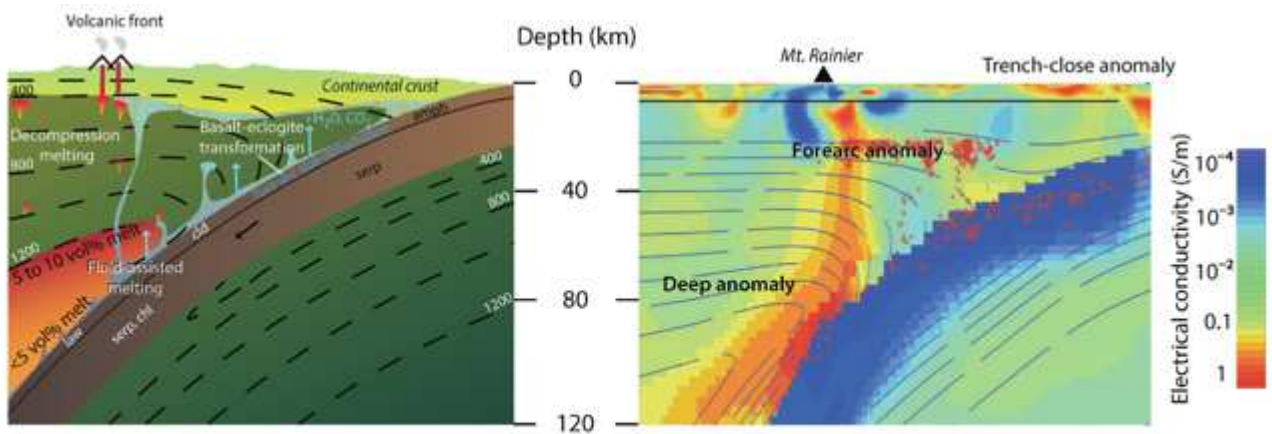


Figure 2. Detection of fluids using electromagnetic studies. Comparison between the petrological view of a subduction zone (left; after Schmidt and Poli, 1998; Grove et al., 2012; Timm et al., 2014) and an electromagnetic profile (right; Cascadia, McGary et al., 2014). Labels in the slab correspond to stable hydrous minerals: amph – amphibole; chl – chlorite; law – lawsonite; serp – serpentine; chl – chlorite. The location of the model profile is shown on the inset map of Figure 6. Dashed lines correspond to isotherms and associated numbers refer to temperature in °C.

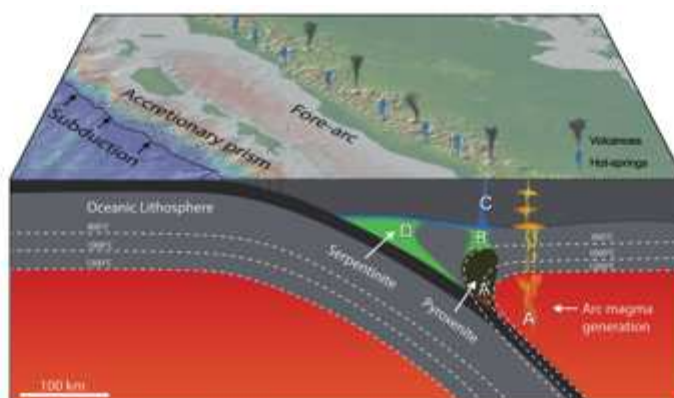


Fig. 2 Subduction zone with fore-arc metasomatism model. Arc magmas form below the volcanic front (**A**), where fluid-fluxed melting of mantle peridotites occurs. In front of the region of arc magma generation (**A'**) subducted sediments melt and their hydrous melts rise and react with peridotite. Since temperatures in front of the arc (**A'**) are below the solidus of peridotite, hydrous sediment melt reacts to form a phlogopite-pyroxenite metasome. Fluids expelled by phlogopite-pyroxenite formation rise through the mantle wedge **B** into the crust **C** to form reservoirs and hot springs. Map modified from GeoMapApp, www.geomapapp.org/ with Global Multi-Resolution Topography (GMRT)⁶⁷.

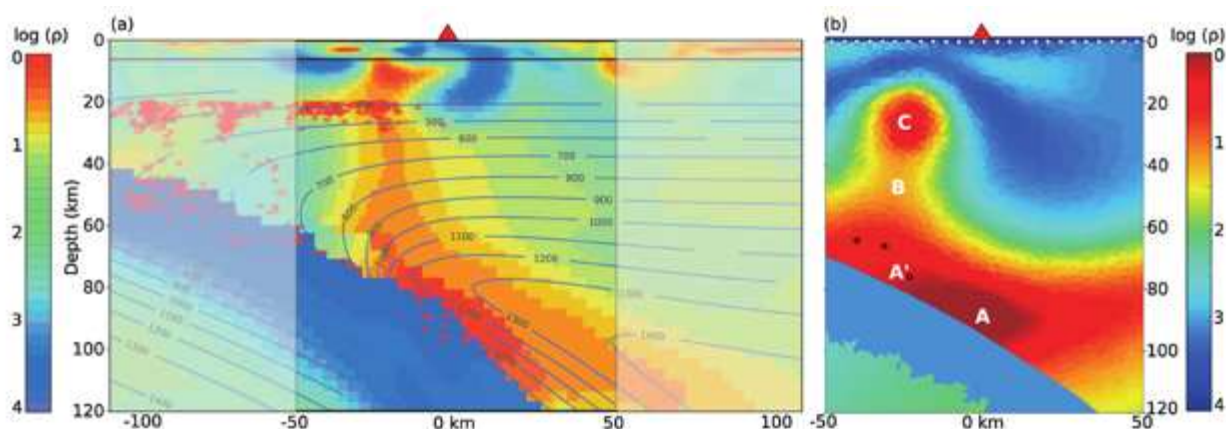


Fig. 3 Original (a) and synthetic (b) MT models for the Cascadia subduction zone. Colour scale is log electrical resistivity (ρ). **a** Shows the inverse MT model along the 'CAFE' line in the Cascadia subduction zone, western North America, adapted from McGary et al¹⁷ with the region of interest highlighted. Reprinted by permission from Springer Nature, Nature, Pathway from subducting slab to surface for melt and fluids beneath Mount Rainier, McGary et al¹⁷, ©2014. **b** is the synthetic MT model, which was created by forward modelling and then inverting the MT responses from a subsurface with conductivities defined by mantle peridotite, arc melts, and the phlogopite-pyroxenite metasome, melt, and saline fluids produced by melting of subducted sediments. The synthetic model reproduces the main conductive features, which are offset trenchward of Mt. Rainier (red triangle). Labels (A, A', B and C) follow the regions labelled in Fig. 2. Black circles in **(b)** show the locations of small (magnitude < 3) earthquakes that have occurred in the mantle wedge since 1980.

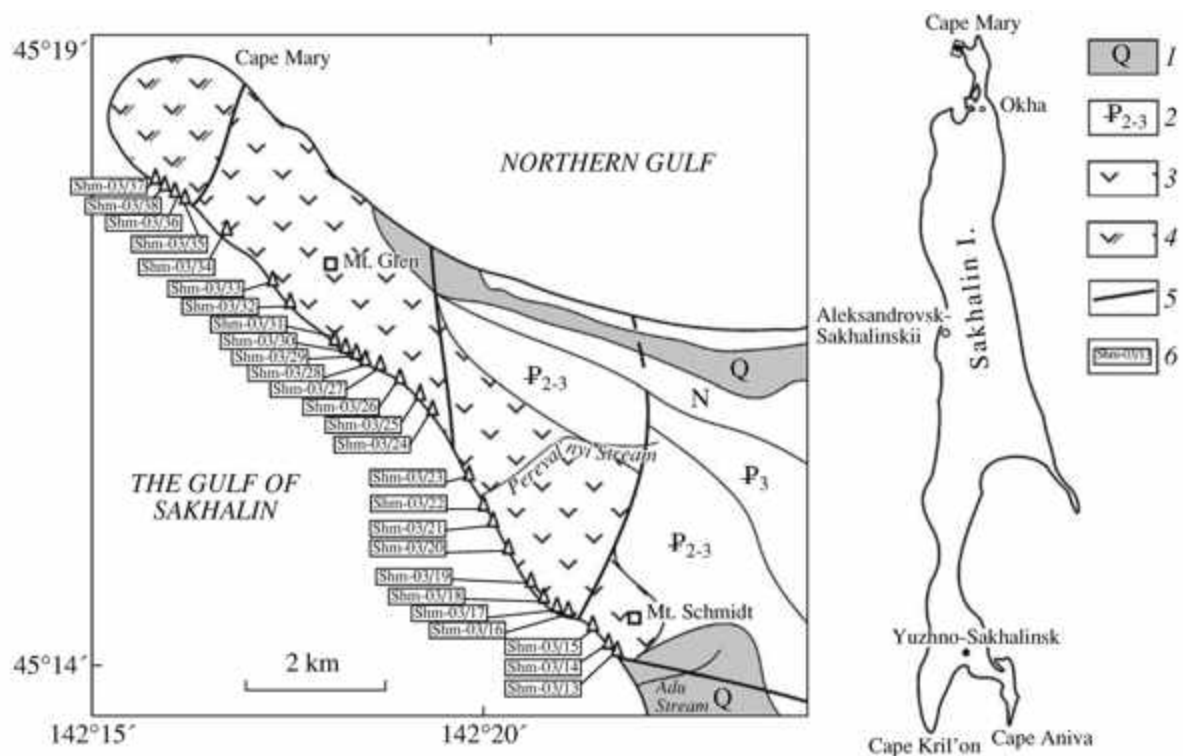


Fig. 1. Sampling localities of the volcanic rocks of the Mariiskiy sequence and vent extrusion of Cape Mary, Schmidt Peninsula. Modified after the GDP-200 map [4]. (1) Quaternary deposits; (2) formations with age indices; (3) early Cretaceous volcanic and volcanogenic-sedimentary rocks of the Mariiskiy sequence; (4) vent extrusions of Cape Mary; (5) fault; (6) number and locality of samples.

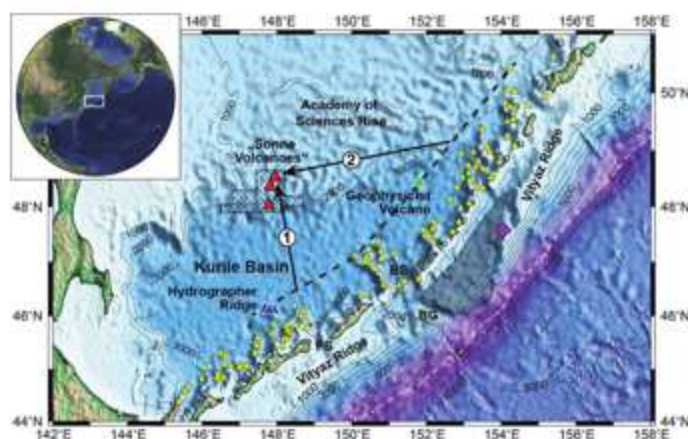


Figure 1. Location of the submarine volcanic edifices in the Kurile Island Arc system: Small yellow triangles indicate volcanoes according to Ardeiko et al. (1992) [14]. Large red triangles mark volcanic edifices discovered during the R/V Sonne cruise SO178 and large dark blue (Hydrographer Ridge) and green (Geophysicist volcano) triangles back arc volcanoes which have been investigated in the framework of the German–Russian KOMEX project. Black dashed line connects young or recent back arc volcanoes located at the greatest distance from the trench axis (white dashed line). Black numbered arrows mark the migration track of the “Sonne Volcano” by spreading in (1) SW–NE directions or (2) NNW–SSE direction (2). Arrows #1 roughly corresponds to the axis of the basement rise in the central part of the Kurile Basin. The dotted polygon indicates the area mapped by multi-beam echo-sounding on SO178. The shaded area marks the extent of a recently discovered fore arc extension structure (e.g., Leškov et al., 2008 [13], Emelyanova et al., 2012 [10]). The purple diamond shows the location of the dredge hauls on the Vityaz Ridge which yielded the trachy-andesite discussed in this study. The base map is from “The GEBCO_2014 Grid, version 20150318, <http://www.gebco.net/>”. Contour interval is 1000 m. BS = Bussol Strait, FS = Frisa Strait, BG = Bussol Graben.

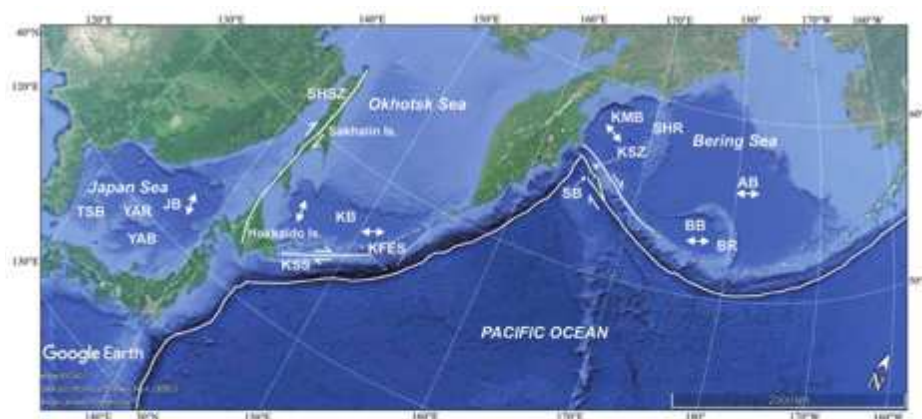


Figure 9. Marginal seas of the NW Pacific and their back arc basins: AB—Aleutian, BB—Bowers, kmB—Komandorsky, KB—Kurile, JB—Japan, YAB—Yamato, TSB—Tsushima. Ridges and rises separating the back arc basins: BR—Bowers, SHR—Shirshov, YAR—Yamato. Extension structures in the Aleutian and Kurile fore arcs: SB—Steller Basin (Baranov et al., 1991 [52]), KFES—Kurile Fore Arc Extension Structure (Laverov et al., 2006 [50]). The white line marks the trench axis, white lines with arrows indicate active shear zones: KSS—Komandorsky (Baranov et al., 1991 [52]), SHSZ—Sakhalin–Hokkaido (Jolivet et al., 1987 [3]), KSS—Kurile Sliver Shear (Kimura 1986 [53]). White lines with arrows at both ends mark the opening direction of the back arc basins. Two opening directions are suggested for the Kurile Basin: NNW–SSE direction in Middle Miocene and NE–SW direction later than Late Miocene (TuZino and Muramaki 2008 [54]).

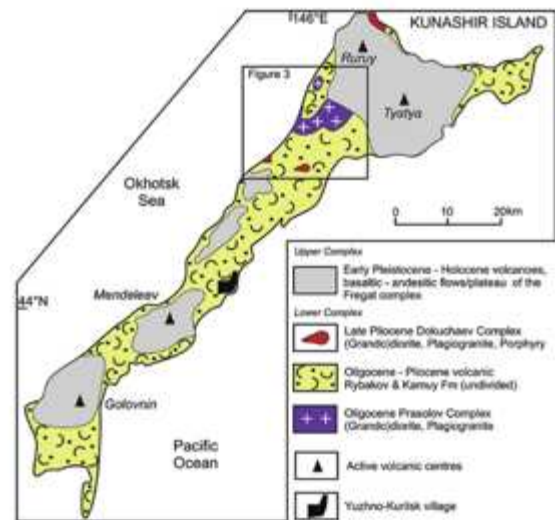


Figure 2. General geological map of Kunashir Island, southwest Kuril Islands (based on Kovtunovich et al., 2002). Location for Fig. 3 is indicated.

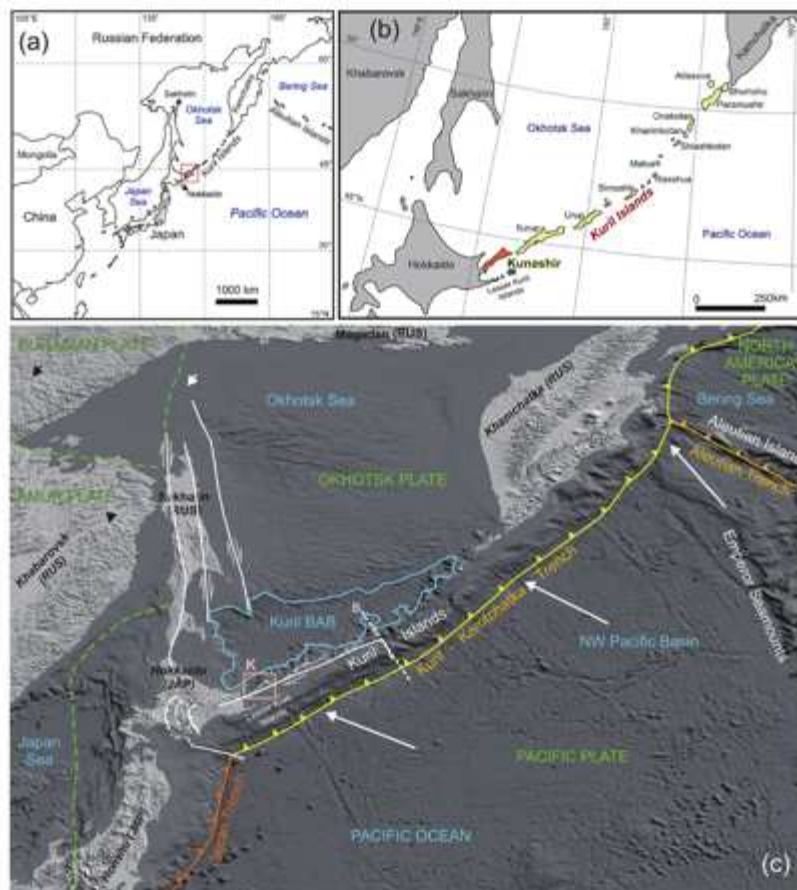
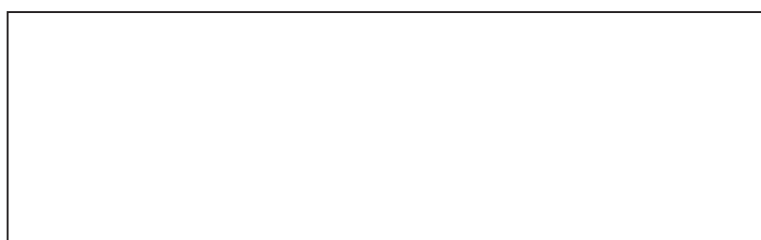


Figure 1. (a) General location of the Kuril Island arc in the Northwest Pacific, (b) position of Kunashir Island in the Kuril arc and general regional geographic setting, and (c) tectonic sketch map of the Kuril island arc. The study area, the island of Kunashir (K), is indicated by the red box.







HOKKAIDO RESEARCH CENTER OF GEOLOGY

〒040-8620 札幌市東区南一条西五丁目

〒040-8620

〒040-8620

〒040-8620